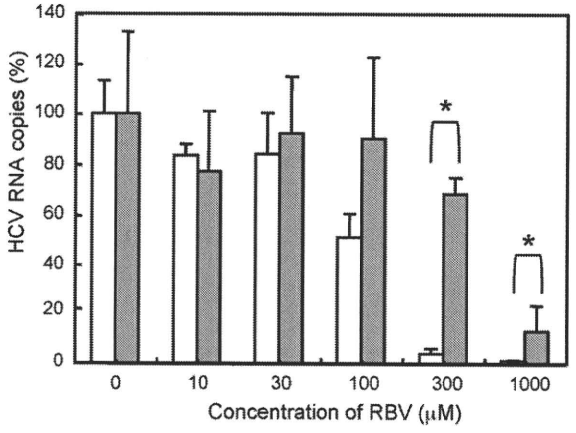


**Fig. 1.** Inhibitory effect of RBV on HCV RNA levels in genotype 2a replicon cells after long-term treatments with RBV. The replicon cells were serially passaged in 0 or 200 μM RBV for 20 weeks. The cells were then split and incubated with fresh RBV at various concentrations in the absence of G418 for 3 days, followed by the determination of HCV RNA. Clear bars, passage in the absence of RBV: gray bars, passage in the presence of RBV. HCV RNA copies per microgram of total RNA were normalized as percentages of those of untreated (RBV 0 μM). Each data point is presented as the mean of three independent determinations with standard deviation. *$p < 0.05$.

cells; the $EC_{50}$ values for the variant and wild-type replicon cells were 470 and 102 μM, respectively (Fig. 1). Comparable cytotoxic effects of RBV were observed against wild-type and variant replicon cells, with the $CC_{50}$ (50% cytotoxicity concentration) values of 151 and 156 μM, respectively (data not shown).

### 3.2. Mapping RBV resistance to cell line or replicon RNA

To test whether reduced susceptibility to RBV in the variant cells observed as above was due to the appearance of mutations within the viral RNA or was cell-derived, total RNAs from the variant and wild-type replicon cells were extracted and used for retransfection of naïve Huh7 cells. Retransfected cells resistant to G418 were established after 4 weeks of cultures in the presence of 1 mg/ml G418 and were assessed for HCV RNA replication sensitivity to RBV (Fig. 2A). HCV RNA levels in the cells obtained from the wild-type replicon were inhibited by 56, 89 and 97% with 100, 300 and 1000 μM RBV, respectively. By contrast, the culture retransfected with RNA derived from the variant replicon cells exhibited inhibition levels of 13, 29 and 89% with the corresponding concentrations of RBV. $EC_{50}$ values were calculated to be 93 and 449 μM, respectively. We confirmed the presence of replicon mutations, as described below, in the cells retransfected with RNA derived from the variant replicon cells.

In order to explore the possibility for cell-derived resistance, both wild-type and variant replicon cells were cured of viral RNAs by IFN treatment; cells were passaged with media containing 100 IU/mL IFN-α in the absence of G418 for 2 months. To compare RBV sensitivity, cured cells were transiently transfected with the wild-type JFH-1 subgenomic replicon RNA and were treated with various concentrations of RBV for 72 h. Similar anti-HCV effects of RBV were observed in the cured cells derived from wild-type and variant replicons, with the $EC_{50}$ values of 147 and 118 μM, respectively (Fig. 2B). Thus, the results suggest that the RBV resistance observed may arise by mutations in the replicon rather than by changes in the cells.

### 3.3. HCV mutations in replicon variant with reduced susceptibility to RBV

It has been reported that mutations in RNA virus genomes responsible for RBV resistance are mostly present in the coding region for the viral RNA-dependent RNA polymerase (RdRp). On the other hand, it is known that RBV works as an RNA mutagen to generate rapidly mutating viral RNA and that NS5B RdRp and other nonstructural proteins in HCV are involved in the viral replication complex, playing key roles in genome replication. Therefore, we sequenced the coding regions for NS3 through NS5B proteins of the replicon molecules in order to determine whether mutations associated with RBV resistance were generated. As shown in Table 2, there were numerically more synonymous and non-synonymous mutations in the RBV-resistant variant replicon cells (RBV treatment) when compared with untreated replicative conditions (No-treatment) across most regions examined. Mutation frequencies of NS3, NS4B and NS5A regions of RBV treatment were significantly higher than those of No-treatment. The total number of synonymous mutations in the RBV-resistant variant replicon cells was 3 times higher than that under untreated replicative conditions, and the number of non-synonymous mutations in the RBV-resistant variant replicon cells was 1.5 times higher than that under untreated replicative conditions. The number of both synonymous and non-synonymous mutations (NS3, NS4B, NS5A and NS5B regions) in the RBV-resistant replicon cells was greater than that in the control cells. We also found a large number of transition

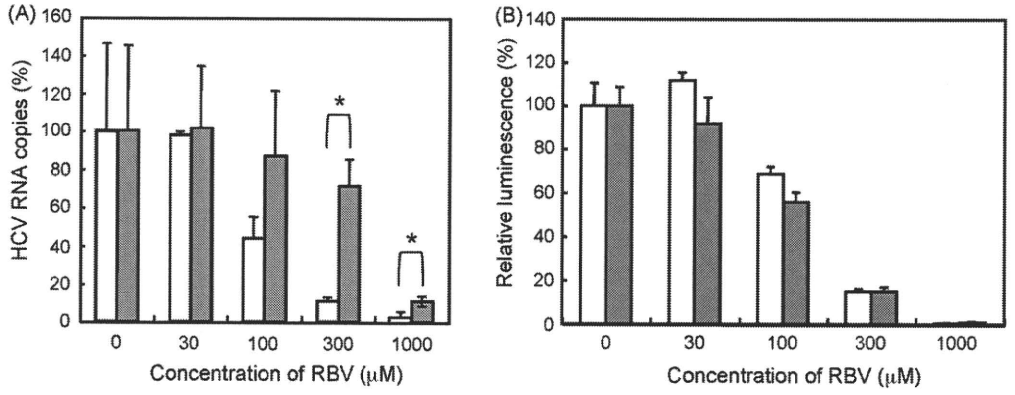


**Fig. 2.** Testing for replicon-derived resistance (A) or for cell-derived resistance (B). (A) Total RNA from RBV-resistant- or wild-type replicon cells was transfected into naïve Huh7 cells. After selection in 1 mg/ml G418 for 4 weeks, re-established replicon cells, wild-type derived (clear bars) and RBV resistance derived (gray bars), were treated with increasing concentrations of RBV in the absence of G418 for 3 days. HCV RNA copies per microgram total RNA were assessed and the levels from wild-type cells without RBV treatment were set at 100%. Data are indicated as means with standard deviations. *$p < 0.05$. (B) RBV-resistant- or wild-type replicon cells were cured by passage in IFN-α in the absence of G418. Cured cells were transiently transfected with the replicon RNA derived from pSGR-JFH1/luc. Transient replication assay of transfectants derived from wild-type (clear bars) and RBV resistance (gray bars) was performed after treatment with various concentrations of RBV for 72 h. The values for wild-type-derived cells without RBV treatment were set at 100%. Data are indicated as means with standard deviations.

**Table 2**
Mutation frequencies in HCV NS regions after 20-weeks culture with or without RBV treatment.

| Region | nt length | No-treatment | | | RBV treatment | | |
|---|---|---|---|---|---|---|---|
| | | No. of non-synonymous mutations[a] | No. of synonymous mutations[a] | Mutation frequency ($10^{-3}$) | No. of non-synonymous mutations[a] | No. of synonymous mutations[a] | Mutation frequency ($10^{-3}$) |
| NS3 | 1893 | 1.7 ± 2.1 | 2.3 ± 1.5 | 2.1 | 4.7 ± 2.4 | 6.5 ± 2.5 | 5.9[b] |
| NS4A | 165 | 1.0 ± 1.0 | 0.3 ± 0.6 | 8.1 | 0.3 ± 0.5 | 0.5 ± 0.9 | 4.4 |
| NS4B | 780 | 1.3 ± 1.2 | 0.3 ± 0.6 | 2.1 | 2.3 ± 1.5 | 2.5 ± 1.2 | 4.7[c] |
| NS5A | 1380 | 4.0 ± 1.2 | 2.0 ± 1.2 | 4.3 | 5.9 ± 1.2 | 6.2 ± 2.4 | 12.2[c] |
| NS5B | 1773 | 4.5 ± 1.5 | 2.3 ± 1.5 | 3.8 | 4.8 ± 1.8 | 4.2 ± 1.1 | 9.0 |
| NS3–NS5B | 5991 | 12.5 ± 2.7 | 7.3 ± 2.7 | – | 17.8 ± 4.5 | 20.1 ± 4.6 | – |

[a] Values are means ± standard deviations.
[b] $p < 0.05$ relative to No-treatment by the unpaired $t$-test.
[c] $p < 0.01$ relative to No-treatment by the unpaired $t$-test.

mutations in RBV-resistant cells, particularly G-to-A and C-to-U transitions, as expected from previous studies. Although mutations were distributed throughout nonstructural regions, four major amino acid substitutions; T1134S in the NS3 region, P1969S in NS4B, V2405A in NS5A, and Y2471H in NS5B, not seen in wild-type cells were observed in most of the subclones among RBV-resistant replicon cells. T1134S, P1969S, V2405A, and Y2471H were present, respectively, in 7 of 11, 6 of 11, 8 of 13, and 7 of 13 PCR subclones sequenced.

### 3.4. Effects of T1134S, P1969S, V2405A, and Y2471H on RBV susceptibility

To test the possibility that any of the four mutations as identified confer resistance to RBV, we introduced these mutations individually into the JFH-1 subgenomic replicon containing a luciferase reporter gene. Cells transfected with mutant- or wild-type replicon RNA grown in the presence of various concentrations of RBV for 2 or 3 days. As demonstrated in Fig. 3A, the replication levels of all four mutant replicons (SGR-JFH1/Luc-T1134S, -P1969S, -V2405A, and -Y2471H) in the presence of 125 or 500 μM RBV were higher than those of the wild-type replicon. In particular, the Y2471H mutant significantly reduced susceptibility to RBV; replication levels of SGR-JFH1/Luc-Y2471H were 3–5-fold higher when compared to those of wild-type under the present assay conditions.

The relative replication activity of these mutant replicons was further determined in 3-day replication assay without drug treatment (Fig. 3B). All mutant replicons exhibited reduced efficiency relative to the wild-type replicon. Levels of the Y2471H-mutated replicon were approximately 30% of those of the wild-type, thus suggesting that replicon mutants with reduced sensitivity to RBV are associated with decreased replication fitness.

## 4. Discussion

It is generally accepted that, during chemotherapy against viral infection, high rates of viral replication and high frequencies of mutation lead to generation of drug-resistant mutants. Although several potential mechanisms for the inhibition of HCV replication by RBV have been proposed, the molecular mechanisms involved in the generation of RBV-resistant HCV remain poorly understood.

This study found that long-term treatment of HCV JFH-1-derived replicon cells with RBV leads to selection of preferential mutations in NS3 (T1134S), NS4B (P1969S), NS5A (V2405A) and NS5B (Y2471H) genes. Each mutation only required a single nucleotide change, and P1969S, V2405A and Y2471H are transition mutations, which are known to be commonly caused by incorporated RBV. Site-directed mutagenesis of these mutations into the replicon demonstrated that Y2471H plays a role in reduced susceptibility to RBV.

Crystal structure information revealed that HCV RdRp is organized into an arrangement with palm, fingers, and thumb subdomains (Lesburg et al., 1999). Residue 2471 (the 33rd position of NS5B) is present in the N-terminal loop region that bridges the fingers. Although this site is apparently distant from the active site of the polymerase in the palm region, it has been reported

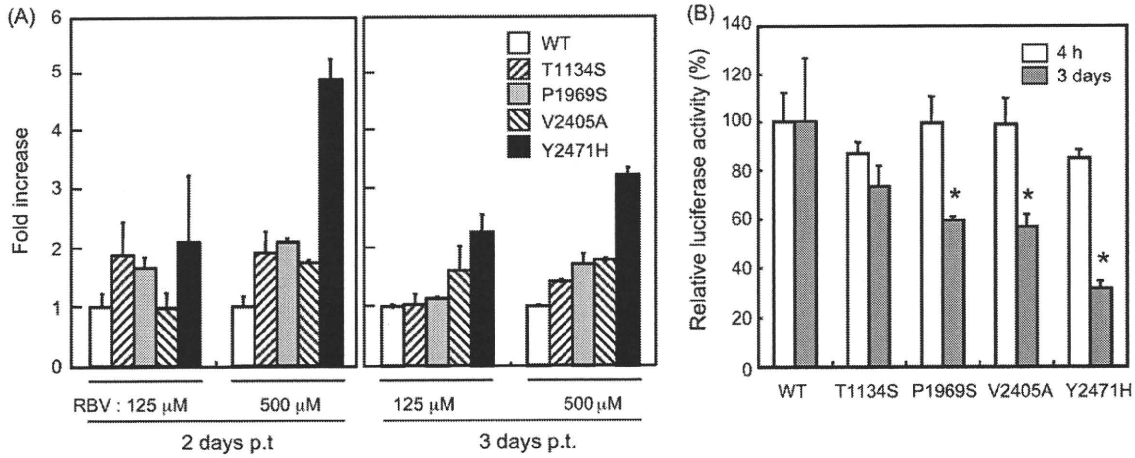


**Fig. 3.** Impact of major mutations in NS3–NS5B regions on RBV susceptibility (A) and replication capacity (B). Mutated replicons carrying single residue substitutions (T1134S, P1969S, V2405A, and Y2471H) were constructed and used for transient replication assay. Cells were transfected with either wild-type (WT) or with mutant replicon RNA in the absence or presence (125, 500 μM) of RBV. Luciferase activity was assessed at 4 h, 2 days and 3 days post-transfection (p.t.). (A) Luciferase activities of WT were set at 1, and the fold increases in the activities of mutants were plotted. (B) Luciferase activities in the absence of RBV at 4 h and 3 days post-transfection were shown. The activities of mutants were normalized as percentages of the WT activities. Data from triplicate samples were averaged and indicated with standard deviations. *$p < 0.05$ against WT.

that small molecules, such as benzimidazole compounds, are able to specifically bind the fingers-thumb interface and inhibit polymerase activity (Herlihy et al., 2008), thus suggesting that amino acid substitutions in the loop region may affect RNA polymerization. The involvement of tyrosine residue at position 415 of HCV NS5B in RBV resistance has been previously described for patients with genotype 1a infection and for the genotype 1b replicon (Young et al., 2003). Although the mechanism for resistance remains elusive, it has been hypothesized that RBV interacts with RdRp around this residue, which is located in the thumb subdomain, thus affecting RNA polymerization (Young et al., 2003).

Based on analysis of available sequences from Genbank, tyrosine at the 33rd residue of NS5B is conserved in all isolates of genotype 2a, but not in other genotypes. In genotype 1a and 1b isolates, 96% contain histidine and only a small population contains tyrosine or asparagine at the site. All the isolates of genotypes 3, 4, 5 and 6 contain histidine, whereas phenylalanine is conserved for genotype 2b. It should be noted that V2405 and P1969 are also completely conserved for genotype 2a but not for other genotypes. Therefore, it is likely that the identified HCV variants with reduced susceptibility to RBV are genotype-specific. It will be of interest to determine whether HCV genotype 2a is intrinsically more sensitive to RBV when compared with other genotypes.

At present, at least 4 mechanisms of action of RBV are proposed (Lau et al., 2002). They include (1) direct inhibition of the HCV replication machinery, (2) as an RNA mutagen that drives a rapidly mutating RNA virus over the threshold to "error catastrophe", (3) inhibition of the host enzyme inosine monophosphate dehydrogenase (IMPDH), and (4) enhancement of host T-cell-mediated immunity against viral infection. In addition to the direct inhibition, it is also possible that other mechanisms such as error-prone and IMPDH-inhibition are involved in HCV escape from RBV treatment. Further investigation of the interaction of HCV variants with the viral and cellular factors involved in viral resistance may improve understanding of the mechanism(s) of RBV resistance.

In conclusion, RBV encountered resistance from the HCV genotype 2a replicon largely mediated by mutations in the N-terminal region of NS5B. Although whether these mutagenic effects are also demonstrable in IFN-RBV combination therapy will require further studies, the mutations identified in this study represent the first drug-resistant variants belonging to HCV genotype 2a. The drug resistance patterns found in this study may be of benefit in prediction in vivo resistance profiles and the development of next-generation nucleoside analogues as anti-HCV drugs.

## Acknowledgments

We thank M. Matsuda, S. Yoshizaki, M. Ikeda, T. Shimoji, M. Kaga and M. Sasaki for their technical assistance. This work was supported by a grant-in-aid for Scientific Research from the Japan Society for the Promotion of Science, from the Ministry of Health, Labour and Welfare of Japan and from the Ministry of Education, Culture, Sports, Science and Technology, and by Research on Health Sciences focusing on Drug Innovation from the Japan Health Sciences Foundation, Japan and by the Program for Promotion of Fundamental Studies in Health Sciences of the National Institute of Biomedical Innovation of Japan. S.S.H. is the recipient of a Research Resident Fellowship from Viral Hepatitis Research Foundation of Japan.

## References

Aizaki, H., Nagamori, S., Matsuda, M., Kawakami, H., Hashimoto, O., Ishiko, H., Kawada, M., Matsuura, T., Hasumura, S., Matsuura, Y., Suzuki, T., Miyamura, T., 2003. Production and release of infectious hepatitis C Virus for human liver cell cultures in the three-dimensional radial-flow bioreactor. Virology 314, 16–25.

aus dem Siepen, M., Oniangue-Ndza, C., Wiese, M., Ross, S., Roggendorf, M., Viazov, S., 2007. Interferon-alpha and ribavirin resistance of Huh7 cells transfected with HCV subgenomic replicon. Virus Res. 125, 109–113.

Date, T., Kato, T., Miyamoto, M., Zhao, Z., Yasui, K., Mizokami, M., Wakita, T., 2004. Genotype 2a hepatitis C virus subgenomic replicon can replicate in HepG2 and IMY-N9 cells. J. Biol. Chem. 279, 22371–22376.

Domingo, E., 1996. Biological significance of viral quasispecies. Viral Hep. Rev. 2, 247–261.

Farci, P., Purcell, R.H., 2000. Clinical significance of hepatitis C virus genotypes and quasispecies. Semin. Liver Dis. 20, 103–126.

Forns, X., Purcell, R.H., Bukh, J., 1999. Quasispecies in viral persistence and pathogenesis of hepatitis C virus. Trends Microbiol. 7, 402–410.

Fried, T.R., Bradley, E.H., Towle, V.R., Allore, H., 2002. Understanding the treatment preferences of seriously ill patients. N. Engl. J. Med. 346, 1061–1066.

Herlihy, K.J., Graham, J.P., Kumpf, R., Patick, A.K., Duggal, R., Shi, S.T., 2008. Development of intragenotypic chimeric replicons to determine the broad-spectrum antiviral activities of hepatitis C virus polymerase inhibitors. Antimicrob. Agents Chemother. 52, 3523–3531.

Kato, T., Date, T., Miyamoto, M., Furusaka, A., Tokushige, K., Mizokami, M., Wakita, T., 2003. Efficient replication of the genotype 2a hepatitis C virus subgenomic replicon. Gastroenterology 125, 1808–1817.

Kato, T., Date, T., Miyamoto, M., Sugiyama, M., Tanaka, Y., Orito, E., Ohno, T., Sugihara, K., Hasegawa, I., Fujiwara, K., Ito, K., Ozasa, A., Mizokami, M., Wakita, T., 2005. Detection of anti-hepatitis C virus effects of interferon and ribavirin by a sensitive replicon system. J. Clin. Microbiol. 43, 5679–5684.

Lau, J.Y., Tam, R.C., Liang, T.J., Hong, Z., 2002. Mechanism of action of ribavirin in the combination treatment of chronic HCV infection. Hepatology 35, 1002–1009.

Lesburg, C.A., Cable, M.B., Ferrari, E., Hong, Z., Mannarino, A.F., Weber, P.C., 1999. Crystal structure of the RNA-dependent RNA polymerase from hepatitis C virus reveals a fully encircled active site. Nat. Struct. Biol. 6, 937–943.

Manns, M.P., McHutchison, J.G., Gordon, S.C., Rustgi, V.K., Shiffman, M., Reindollar, R., Goodman, Z.D., Koury, K., Ling, M., Albrecht, J.K., 2001. Peginterferon alfa-2b plus ribavirin compared with interferon alfa-2b plus ribavirin for initial treatment of chronic hepatitis C: a randomised trial. Lancet 358, 958–965.

Martell, M., Esteban, J.I., Quer, J., Genesca, J., Weiner, A., Esteban, R., Guardia, J., Gomez, J., 1992. Hepatitis C virus (HCV) circulates as a population of different but closely related genomes: quasispecies nature of HCV genome distribution. J. Virol. 66, 3225–3229.

Miyamoto, M., Kato, T., Date, T., Mizokami, M., Wakita, T., 2006. Comparison between subgenomic replicons of hepatitis C virus genotypes 2a (JFH-1) and 1b (con1 NK5.1). Intervirology 49, 37–43.

Pfeiffer, J.K., Kirkegaard, K., 2005. RBV resistance in hepatitis C virus replication containing cells conferred by changes in the cell line or mutations in the replicon RNA. J. Virol. 79, 2346–2355.

Simmonds, P., Gallin, J.I., Farrei, A.S., 2000. Hepatitis C virus genotypes. Biomed. Res. Rep. 2, 53–70.

Takeuchi, T., Katsume, A., Tanaka, T., Abe, A., Inoue, K., Tsukiyama Kohara, K., Kawaguchi, R., Tanaka, S., Kohara, M., 1999. Real-time detection system for quantification of Hepatitis C virus genome. Gastroenterology 116, 636–642.

Tanaka, Y., Sakamoto, N., Enomoto, N., Kurosaki, M., Ueda, E., Maekawa, S., Yamashiro, T., Nakagawa, M., Chen, C.-H., Kanazawa, N., Kakinuma, S., 2004. Synergistic inhibition of intracellular hepatitis C virus replication by combination of ribavirin and interferon-alpha. J. Infect. Dis. 189, 1129–1139.

World Health Organization (WHO), 2000. Hepatitis C: global prevalence (update). Weekly Epidemiological Record, WHO 75, 18–19.

Young, K.C., Lindsay, K.L., Lee, K.J., Liu, W.C., He, J.W., Milstein, S.L., Lai, M.M., 2003. Identification of a ribavirin-resistant NS5B mutation of hepatitis C virus during ribavirin monotherapy. Hepatology 38, 869–878.

Zhou, S., Liu, R., Baroudy, B.M., Malcolm, B.A., Reyes, G.R., 2003. The effect of ribavirin and IMPDH inhibitors on hepatitis C virus subgenomic replicon RNA. Virology 310, 333–342.

frontiers in
MICROBIOLOGY

ORIGINAL RESEARCH ARTICLE
published: 08 December 2010
doi: 10.3389/fmicb.2010.00128

# Characterization of natural killer cells in tamarins: a technical basis for studies of innate immunity

**Tomoyuki Yoshida[1,2†], Akatsuki Saito[2,3†], Yuki Iwasaki[1,4], Sayuki Iijima[1], Terue Kurosawa[1], Yuko Katakai[5], Yasuhiro Yasutomi[6], Keith A. Reimann[7], Toshiyuki Hayakawa[2] and Hirofumi Akari[1,2]***

[1] Tsukuba Primate Research Center, National Institute of Biomedical Innovation, Tsukuba, Ibaraki, Japan
[2] Primate Research Institute, Kyoto University, Inuyama, Aichi, Japan
[3] International Research Center for Infectious Diseases, The Institute of Medical Science, The University of Tokyo, Minato-ku, Tokyo, Japan
[4] Graduate School of Medicine and Dentistry, Tokyo Medical and Dental University, Bunkyo-ku, Tokyo, Japan
[5] Corporation for Production and Research of Laboratory Primates, Tsukuba, Ibaraki, Japan
[6] Laboratory of Immunoregulation and Vaccine Research, Tsukuba Primate Research Center, National Institute of Biomedical Innovation, Tsukuba, Ibaraki, Japan
[7] Division of Viral Pathogenesis, Beth Israel Deaconess Medical Center, Harvard Medical School, Boston, MA, USA

**Edited by:**
Yasuko Yokota, National Institute of Infectious Diseases, Japan

**Reviewed by:**
Koji Ishii, National Institute of Infectious Diseases, Japan
Ikuo Shoji, Kobe University Graduate School of Medicine, Japan

***Correspondence:**
Hirofumi Akari, Primate Research Institute, Kyoto University, Inuyama, Aichi 484-8506, Japan.
e-mail: akari@pri.kyoto-u.ac.jp

†Tomoyuki Yoshida and Akatsuki Saito have contributed equally to this work.

Natural killer (NK) cells are capable of regulating viral infection without major histocompatibility complex restriction. Hepatitis C is caused by chronic infection with hepatitis C virus (HCV), and impaired activity of NK cells may contribute to the control of the disease progression, although the involvement of NK cells *in vivo* remains to be proven. GB virus B (GBV-B), which is genetically most closely related to HCV, induces acute and chronic hepatitis upon experimental infection of tamarins. This non-human primate model seems likely to be useful for unveiling the roles of NK cells *in vivo*. Here we characterized the biological phenotypes of NK cells in tamarins and found that depletion of the $CD16^+$ subset *in vivo* by administration of a monoclonal antibody significantly reduced the number and activity of NK cells.

**Keywords: CD16, cynomolgus monkey, tamarin, NK cell**

## INTRODUCTION

Natural killer (NK) cells are a component of the innate immune system that play a central role in host defense against viral infection and tumor cells. Much of the evidence for a role for NK cells in controlling viral infections has come from experiments with mice that were genetically modified (Lian and Kumar, 2002) or were treated with NK cell-depleting antibodies (Kasai et al., 1980) or from the study of humans with inherited NK cell deficiencies (Biron et al., 1989; Orange, 2002).

NK cells can be rapidly recruited into infected organs and tissue by chemoattractant factors produced by virus-infected cells and activated resident macrophages, which are also a major source of interferon (IFN) that induces NK cell proliferation, NK cell-mediated cytolysis of virus-infected cells, and the secretion of chemokines (Robertson, 2002). NK cells can kill virus-infected cells by using cytotoxic granules or by recognizing and inducing lysis of antibody-coated target cells (antibody-dependent cell cytotoxicity) via antibody binding receptor CD16. For instance, human blood NK cells are cytotoxic against dengue virus-infected cells in target organs via direct cytolysis and antibody-dependent cell-mediated cytotoxicity (reviewed by Navarro-Sánches et al., 2005). Early activity of NK cells may be important for clearing acute infections such as that of dengue virus. However, the effect that NK cells may exert on chronic infections with viruses such as hepatitis C virus (HCV) is less clear.

HCV is the causative agent of chronic hepatitis C, cirrhosis, and finally liver cancer. In general, acquired and innate immunity induced by acute HCV infection is not sufficient for the viral clearance, and persistent HCV infection frequently leads to progression to chronic hepatitis (reviewed by Cheent and Khakoo, 2010). It was reported that dendritic cells (DCs) in HCV infection were not responsive to IFN-α, and thus failed to promote subsequent activation of NK cells as a primary innate immune response (reviewed by Kanto, 2008). This is in agreement with the finding that the killing activity of NK cells in patients with chronic hepatitis C is inactivated in *in vitro* studies (Deignan et al., 2002; Golden-Mason et al., 2008). These data suggest that the dysfunction of NK cells contributes to the persistent infection of HCV and chronic hepatitis. On the other hand, it was suggested that inappropriately activated NK cells caused liver injury after the viral infection (Liu et al., 2000). The population of NK cells is relatively minor in peripheral lymphoid organs but is abundant in liver, raising a question as to their function in the innate immune response to acute and chronic HCV infection in the liver. It is possible that NK cells partially regulate the replication of HCV in this organ during early infection whereas they promote the liver dysfunction in chronic HCV infection. To examine these possibilities, it is necessary to clarify the involvement of NK cells *in vivo* in HCV infection. However, it is questionable whether the results of *ex vivo* analyses of NK cells would reflect their actual roles *in vivo*. Therefore, it might be more informative to study the function of NK cells directly by means of *in vivo* depletion technique in animal models.

A chimpanzee model of HCV infection has frequently been employed to evaluate the role of acquired antiviral immune responses, although the involvement of NK cells has not been fully evaluated because of the limitations on the use of chimpanzees

due to ethical and financial restrictions (Cohen and Lester, 2007). Accordingly, New World monkeys infected with GB virus B (GBV-B) appear to be a promising model because (i) among viruses so far known, GBV-B is genetically most closely related to HCV and can infect New World monkeys, including tamarins, marmosets and owl monkeys, but not Old World monkeys (reviewed by Akari et al., 2009), (ii) tamarins develop acute and chronic hepatitis after experimental GBV-B infection (Bukh et al., 1999; Sbardellati et al., 2001; Lanford et al., 2003; Martin et al., 2003; Ishii et al., 2007; Takikawa et al., 2010), (iii) the infection induces antiviral cellular immune responses (Woollard et al., 2008), and (iv) tamarins and marmosets are commercially available and easily handled, reared and bred. Moreover, tamarins, being primates, may have a similar immune system to humans, and therefore they may be useful for studying the function of NK cells against the hepatitis virus in this tamarin model.

Our final goal is to study the role of NK cells as a major player in innate immunity during the course of the progression of viral hepatitis. Since some basic information regarding the biological characteristics of NK cells still remains unclear, we initially sought to characterize NK cells in tamarins to provide a technical basis for further studies.

## MATERIALS AND METHODS

### ANIMALS

Five red-handed tamarins (*Saguinus midas*) and five cynomolgus monkeys (*Macaca fascicularis*) were used in this study. The animals were cared for in accordance with National Institute of Biomedical Innovation rules and guidelines for experimental animal welfare, and all protocols were approved by our Institutional Animal Study Committee.

### FLOW CYTOMETRY

Flow cytometry was performed as previously described (Akari et al., 1997) with a slight modification. Fifty microliters of whole blood from cynomolgus monkeys and tamarins was stained with combinations of fluorescence-conjugated monoclonal antibodies (mAb): anti-CD3 (SP34-2; Becton Dickinson), anti-CD4 (L200; BD Pharmingen), anti-CD8 (CLB-T8/4H8; Sanquin), anti-CD16 (3G8; BD Pharmingen), and anti-CD16 (DJ130c; Dako). Then, erythrocytes were lysed with FACS lysing solution (Becton Dickinson). After having been washed with sample buffer containing phosphate-buffered saline (PBS), 1% fetal calf serum (FCS), and 1% formaldehyde, the labeled cells were resuspended in the sample buffer. The expression of the immunolabeled molecules on the lymphocytes was analyzed with a FACSCanto II flow cytometer (Becton Dickinson). Peripheral blood mononuclear cells (PBMCs) were separated from the blood of these monkeys by a Ficoll-Paque gradient method. The cells were resuspended in complete medium composed of RPMI-1640 medium supplemented with 10% FCS, 1% penicillin/streptomycin, 2 mM HEPES and 55 μM 2-mercaptoethanol at 4°C until use. Fluorochrome-labeled mouse mAbs were reacted with $2 \times 10^5$ PBMCs at 4°C for 30 min. The labeled cells were washed with PBS containing 1% FCS, and resuspended in the sample buffer. The expression of the immunolabeled molecules on the lymphocytes was analyzed as mentioned above.

### FLOW CYTOMETRIC 5-(AND 6)-CARBOXYFLUORESCEIN DIACETATE SUCCINIMIDYL ESTER (CFSE)/7-AMINO ACTINOMYCIN D (7-AAD) CYTOTOXIC ASSAY

Peripheral blood mononuclear cells were separated from the blood of these monkeys by a Ficoll-Paque gradient method. These PBMCs were then resuspended in complete medium at 37°C until use. The flow cytometric CFSE/7-AAD cytotoxicity assay was performed as previously described (Lecoeur et al., 2001) with slight modifications. K562 cells ($3 \times 10^6$) were labeled with 500 nM CFSE (from a 1 mM stock solution in dimethyl sulfoxide [Sigma] stored at −20°C) in Hanks' Balanced Salt Solution for 8 min at 37°C in total of 2 ml. The cells were then washed twice in complete medium and used immediately for the cytotoxicity assay. The CFSE-labeled target cells (20,000 cells) were used at different E (effector):T (target) ratios (0:1, 3:1, and 9:1). After 24 h incubation, the cells were stained with 0.25 μg/ml of 7-AAD and incubated for 10 min at 37°C in a $CO_2$ incubator. The cells were washed twice with 1% FCS–PBS, resuspended in sample buffer and analyzed immediately by flow cytometry.

### MAGNETIC CELL SEPARATION

Magnetic cell separation (MACS) was performed as previously described (Tenorio and Saavedra, 2005) with slight modifications. PBMCs ($1 \times 10^7$) were washed with 3 ml of MACS buffer composed of PBS with 2 mM EDTA and 0.5% bovine serum albumin, and resuspended in 100 μl of the same buffer. Ten microliters of fluorescein isothiocyanate (FITC)-labeled anti-CD16 mAb (3G8) was added. The cells with or without the mAb were incubated for 10 min at 4°C, washed with 1 ml of MACS buffer, and resuspended in 80 μl of the same buffer. They were mixed with 20 μl of anti-FITC MicroBeads and incubated for 15 min at 4°C, washed with 1 ml of MACS buffer, and resuspended in 500 μl of the same buffer. The CD16-positive cells were separated by negative selection using LD columns and a MACS separation unit following the instructions provided by the manufacturer (Miltenyi Biotec). CD16-negative cells were resuspended in complete medium and co-cultured with K562 cells at 37°C for the NK cytotoxicity assay immediately.

### DETECTION OF CIRCULATING ANTI-CD16 MAB (3G8)

Concentrations of an anti-CD16 antibody (3G8) in plasma samples were assessed using a mouse $IgG_1$ Quantitative ELISA Kit (Bethyl Laboratory, Inc.). The assay was performed according to the manufacturer's instruction with a slight modification. To detect the mAb in monkey plasma, 96-well enzyme-linked immunosorbent assay (ELISA) plates were coated with a capture antibody and incubated for 1 h at 37°C and washed with wash solution (50 mM Tris, 0.14 M NaCl, 0.05% Tween 20, pH 8.0) three times. The plates were blocked with blocking solution (Postcoat) for 30 min at 37°C. Plasma samples from antibody-treated monkeys were diluted in dilution buffer (50 mM Tris, 0.14 M NaCl, 1% bovine serum albumin, 0.05% Tween 20, pH 8.0), applied to the wells in serial dilutions, incubated for 1 h at 37°C and washed with the wash solution five times. Goat anti-mouse $IgG_1$ conjugated with horseradish peroxidase and diluted 1:50000 in dilution buffer was added to each well and incubated for 1 h at 37°C. Each well was washed with the wash solution five times. Substrate solution was added to each well and incubated

for 10–15 min at room temperature, and then the reaction was stopped with $H_2SO_4$. Optical density was measured using an ELISA reader at 450 nm.

### *IN VIVO* DEPLETION OF CD16 POSITIVE CELLS

Mouse anti-human CD16 (3G8) mAb (Fleit et al., 1982) was produced in serum-free medium and purified using protein A affinity chromatography. Endotoxin levels were lower than 1 EU/mg. The antibody was administered to tamarins (Tm 05-003, Tm 06-020) and cynomolgus monkeys (Mf 00-005, Mf 99-110) intravenously at 50 mg/kg at a rate of 18 ml/min using a syringe pump. Lymphocyte subsets were monitored for 3 weeks after the administration.

### STATISTICAL ANALYSIS

Statistical analyses of lymphocyte ratios were performed using Student's *t*-test and single-factor ANOVA, followed by Fisher's protected least-significant difference *post hoc* test by using StatView software (SAS Institute, NC, USA). The results were confirmed in more than three independent experiments in tamarins and cynomolgus monkeys.

## RESULTS

### LYMPHOCYTE SUBSETS IN TAMARINS

First, we examined the lymphocyte subsets in tamarins as compared with cynomolgus monkeys (**Figure 1**). The percentages of T and B lymphocytes indicated as $CD20^-CD3^+$ and $CD20^+CD3^-$ subsets in the total lymphocytes were found to be 68.8% (range 41.9–68.8%) and 12.3% (range 11.8–12.6%) in tamarins and 68.4% (range 42.6–68.4%) and 10.2% (range 9.1–11.4%) in cynomolgus monkeys, respectively. The percentage of $CD4^+$ T cells in the $CD3^+$ subset was 45.5% (range 41.9–52.5%) and 55.3% (range 42.6–64.4%) while that of $CD8^+$ T cells was 41.0% (range 35.8–44.5%) and 31.2% (range 29.3–34.6%) in tamarins and cynomolgus monkeys, respectively. Next, the NK cell subset was determined as $CD3^-$ $CD16^+$ lymphocytes in this study. The percentage of NK cells was 30.5% (range 16.9–52.5%) and 18.9% (range 13.7–22.4%) in tamarins and cynomolgus monkeys, respectively. We analyzed statistically whether these lymphocyte ratios were different between tamarins and cynomolgus monkeys, and found that there were no significant differences of the lymphocyte ratios between them. We therefore concluded that the proportions of the major lymphocyte subsets in tamarins were relatively similar to those in cynomolgus monkeys.

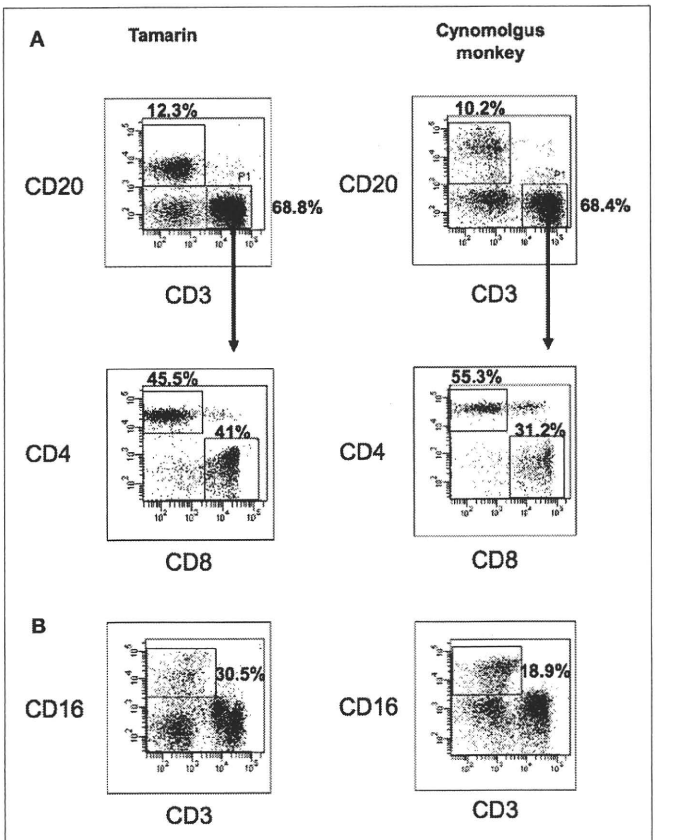


**FIGURE 1 | Flow cytometric analysis of CD3, CD20, CD4, CD8, and CD16 expression on lymphocytes in cynomolgus monkeys and tamarins.** Representative results in tamarins and cynomolgus monkeys are shown. **(A)** Flow cytometric analysis of CD3 and CD20 expression in lymphocytes (top panels) and CD4 and CD8 expression in $CD3^+$ population (bottom panels) of both monkeys. **(B)** Flow cytometric analysis of CD3 and CD16 expression in both monkey species. The numbers denote the percentages of lymphocytes. We analyzed statistically whether these lymphocyte ratios were different between tamarins and cynomolgus monkeys by using StatView software. There were no significant differences of the lymphocyte ratios between them.

### FLUORESCENCE-BASED *IN VITRO* ASSAY FOR QUANTITATIVELY EVALUATING NATURAL KILLER ACTIVITY

Natural killer cell cytotoxic assays conventionally require considerable numbers of PBMCs, and this has been a major hurdle for analyzing the NK activity in small New World monkeys due to the limited availability of their blood. Therefore, we employed an alternative method using a fluorescence-based assay to assess the activity of NK cells in tamarins as previously described (Lecoeur et al., 2001) with slight modifications. When CFSE-stained K562 target cells were incubated with the effector PBMCs obtained from tamarins at an effector/target (E/T) ratio of 9:1, 42% of the K562 cells were positive for 7-AAD, which stains apoptotic cells (**Figure 2A**). We confirmed that the killing activity of NK cells was dose-dependent, and that the level in tamarins was higher than that in cynomolgus monkeys (**Figures 2B and 3**).

Next, in order to examine if $CD16^+$ lymphocytes represent a major population with NK activity, $CD16^-$ PBMCs were obtained by negative selection using MACS (**Figure 4A**) in both tamarins and cynomolgus monkeys. We found that depletion of $CD16^+$ cells greatly attenuated the killing activity in both tamarins and cynomolgus monkeys (**Figure 4B**), indicating that $CD16^+$ lymphocytes are a major population with NK activity.

### *IN VIVO* DEPLETION OF $CD16^+$ NK CELLS USING A MURINE ANTI-CD16 MAB

We next sought to establish a system to directly evaluate the role of NK cells in tamarins. We asked if the administration of an anti-CD16 (3G8) mAb could deplete $CD16^+$ lymphocytes *in vivo*. Tamarins were intravenously administered 3G8 or control mAb (MOPC-21) at a dose of 50 mg/kg. Using an anti-CD16 antibody that is not cross-blocked by 3G8 (clone DJ130c), it was found that at

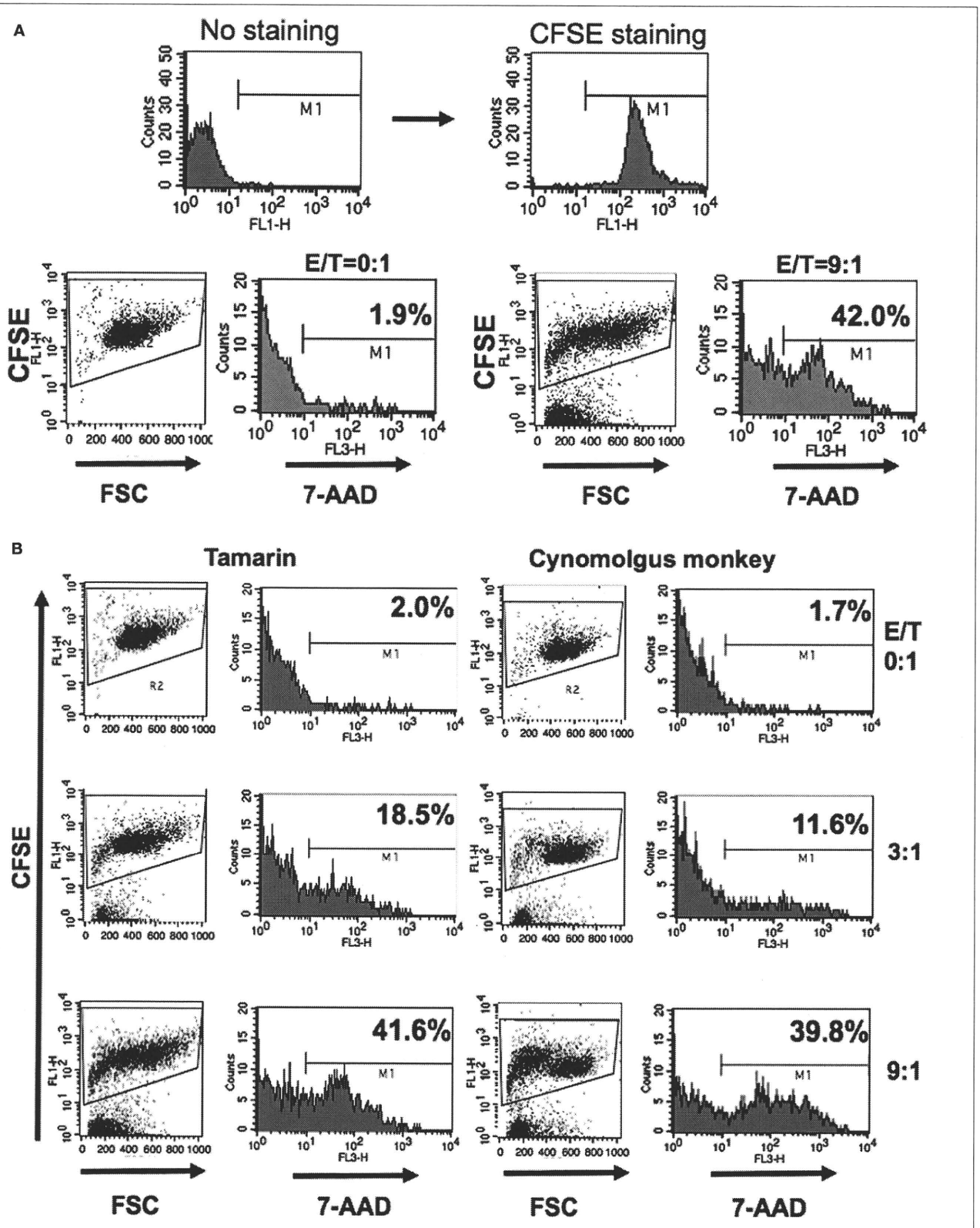


**FIGURE 2 | Cytotoxicity assay by CFSE and 7-AAD staining. (A)** CFSE-stained K562 cells were co-cultured with PBMCs at E/T ratios of 9:1 and 0:1. The CFSE-stained K562 cells were first gated by FSC and SSC characteristics, and 3000 events were captured. **(B)** CFSE-stained K562 target cells were killed by tamarin PBMCs using E/T ratios of 9:1, 3:1, and 0:1. The numbers in the panels denoted the percentages of 7-AAD positive cells. We analyzed statistically whether these killing activities were different between tamarins and cynomolgus monkeys by using StatView software.

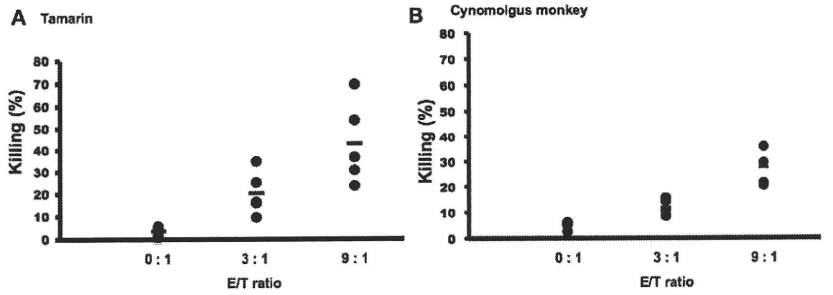


**FIGURE 3 | Dose-dependency of killing activity of NK cells in tamarins. (A,B)** K562 target cells were stained with CFSE and co-cultured with PBMCs as described in Section "Materials and Methods". CFSE-stained K562 target cells were killed by PBMCs of tamarins and cynomolgus monkeys in a dose-dependent manner. For all experiments, the number of observations used to calculate the mean were $n = 5$. We analyzed statistically whether these killing activities were different between tamarins and cynomolgus monkeys by using StatView software.

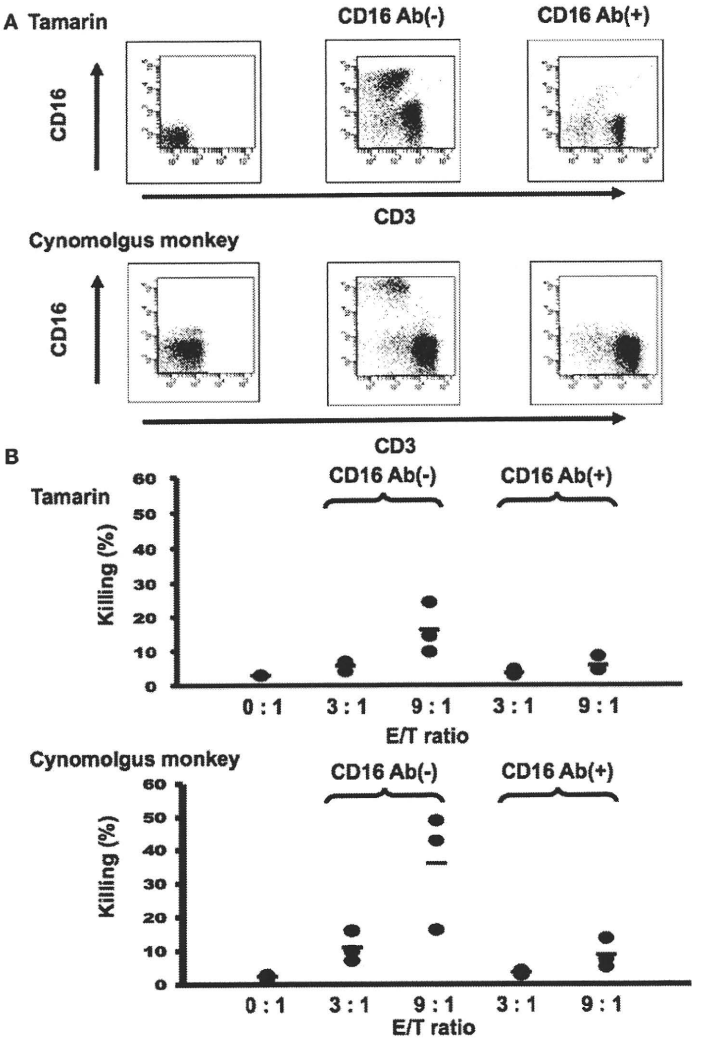


**FIGURE 4 | CD16⁺ cells were a major population with natural killer activity in tamarins. (A)** CD16⁺ cells were depleted from PBMCs by MACS as described in Section "Materials and Methods". CD16⁻ PBMCs were obtained by negative selection using MACS. **(B)** K562 cells were stained with CFSE and co-cultured with CD16-treated or untreated PBMCs as described in Section "Materials and Methods". Results shown are representative of three independent experiments.

1–3 days after the treatment CD16$^+$ cells were completely depleted, followed by recovery to the initial levels at around 2 weeks after the administration, which was consistent with the results in cynomolgus monkeys (**Figure 5B**). It is noteworthy that the numbers of CD4$^+$/CD8$^+$ T and B lymphocytes were not affected by the treatment and that administration of control antibody did not deplete CD16$^+$ cells during the period tested (data not shown), showing that the effect of 3G8 on CD16$^+$ cells was specific (data not shown). We also measured the concentration of the 3G8 mAb in the plasma of antibody-treated monkeys. As shown in **Figure 6**, the concentration of 3G8 reached a plateau at day 1, followed by a gradual decrease in both tamarins and cynomolgus monkeys, which was consistent with the kinetics of CD16$^+$ cells. In the case of MOPC-21 administration to tamarins, similar kinetics of its concentration with that of 3G8 were observed (data not shown).

### ATTENUATION OF CD16$^+$ NK CELL FUNCTION BY *IN VIVO* DEPLETION OF CD16$^+$ CELLS

Finally, we tested whether depletion of the CD16$^+$ subset could attenuate the NK activity in PBMCs. The killing activity was reduced at day 1 and the reduction persisted for 1 week post-treatment in the 3G8-treated monkeys (**Figure 7**). These results showed that the administration of the 3G8 mAb significantly influenced the number and activity of CD16$^+$ lymphocytes in both tamarins and cynomolgus monkeys.

## DISCUSSION

In this study, we attempted to establish a technical basis for the study of NK cells in tamarins. First, we characterized the NK cells in tamarins and showed that the anti-CD16 (3G8) mAb, an NK marker, cross-reacted with the PBMCs (**Figure 1**). Second, we assessed the killing activity of the CD16$^+$ NK cells in tamarins using our improved method (**Figures 2–4**) and demonstrated that CD16$^+$ NK cells were likely to be a major population with the killing activity in tamarins. Finally, to directly examine the role of CD16$^+$ NK cells *in vivo*, we assessed the effect of anti-CD16 (3G8) mAb *in vivo*. After administration of the mAb, CD16$^+$ NK cells were completely depleted and the killing activity was substantially attenuated in the treated monkeys (**Figures 5 and 7**). Our results suggest that our method for depletion of CD16$^+$ NK cells *in vivo* is useful for investigating the pivotal role of NK cells in the response against hepatitis viruses.

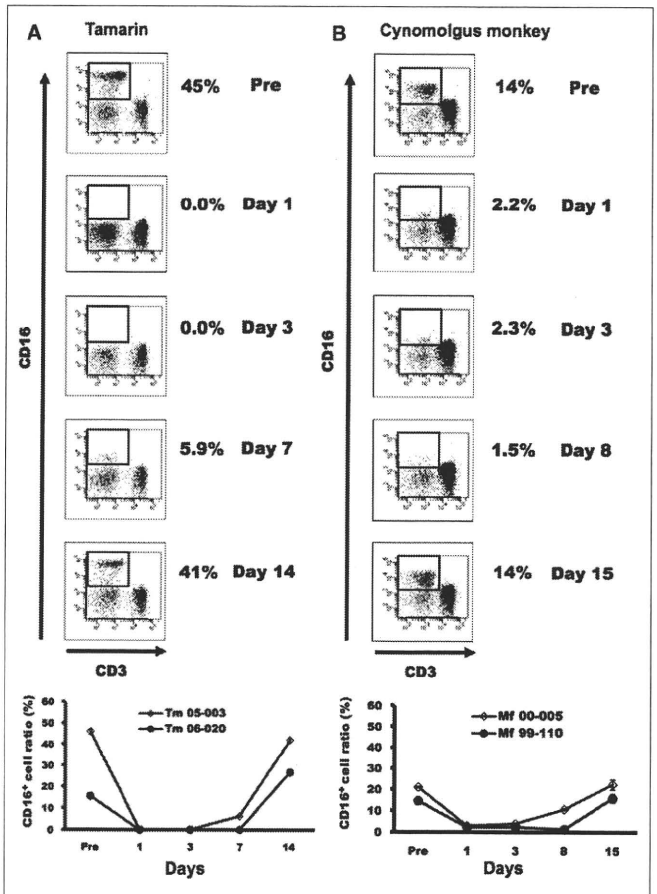


**FIGURE 5 | *In vivo* depletion of CD16$^+$ NK cells using a murine anti-CD16 (3G8) mAb in tamarins. (A,B)** Tamarins and cynomolgus monkeys were administered with 50 mg/kg of the 3G8 mAb. CD16$^+$ NK cell numbers were determined in whole blood specimens. Tamarins: Tm 05-003 and Tm 06-020. Cynomolgus monkeys: Mf 00-005 and Mf 99-110.

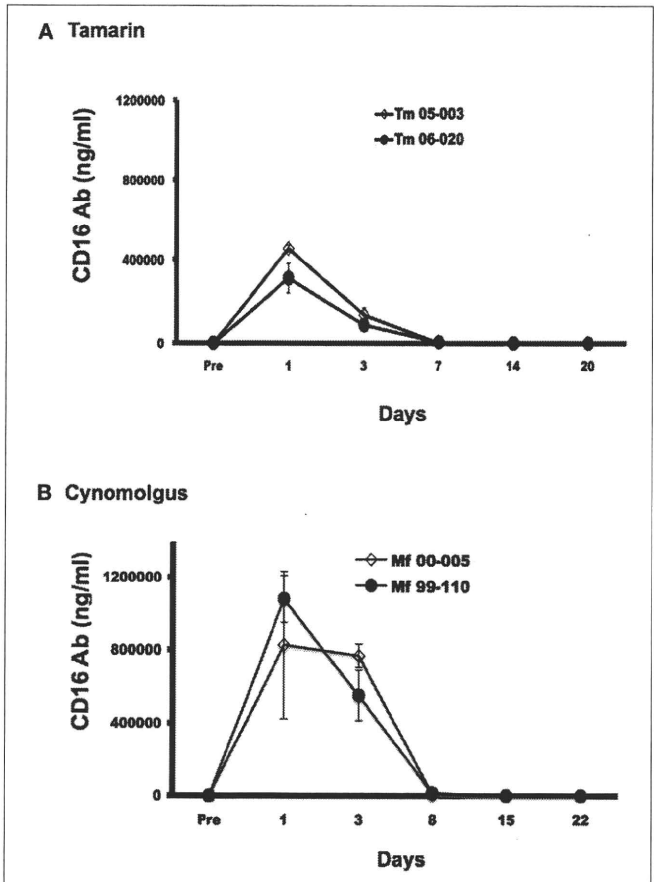


**FIGURE 6 | Kinetics of concentration of CD16 (3G8) mAb *in vivo*.** The concentration of CD16 (3G8) mAb in plasma was measured by ELISA as described in Section "Materials and Methods". Results shown are representative of three independent experiments. **(A)** Tamarins: Tm 05-003 and Tm 06-020. **(B)** Cynomolgus monkeys: Mf 00-005 and Mf 99-110.

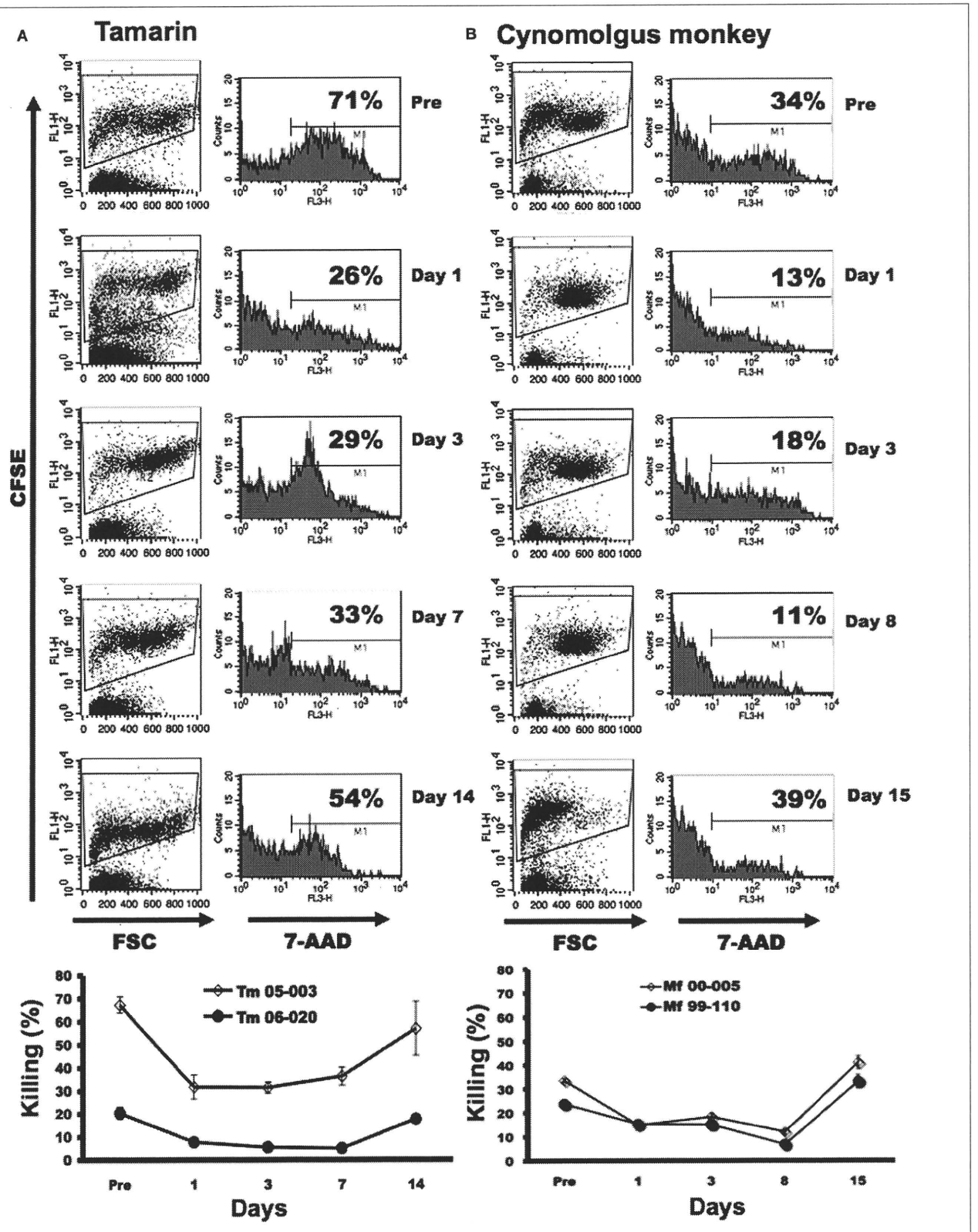


**FIGURE 7 | Attenuation of natural killer activity by *in vivo* depletion of CD16⁺ cells. (A,B)** Tamarins and cynomolgus monkeys were administered 50 mg/kg of murine 3G8 mAb. The activity was determined in PBMCs of both monkeys. Tamarins: Tm 05-003 and Tm 06-020. **(B)** Cynomolgus monkeys: Mf 00-005 and Mf 99-110.

Generally it is impossible to monitor the immunological status in humans pre- and post-infection with hepatitis viruses and to deplete specific subsets such as NK cells *in vivo*. Non-human primates have immune systems similar to that of humans and are suitable for the evaluation of innate and adaptive immune responses against hepatitis viruses (Woollard et al., 2008). GBV-B is most closely related to HCV. Since experimental infection with GBV-B induces acute and chronic hepatitis in tamarins, this model may be useful for the study of antiviral immunity. Moreover, we have also been developing a chimeric virus between HCV and GBV-B. Therefore, if the HCV/GBV-B chimeric virus is able to infect and replicate in tamarins, our method for *in vivo* depletion of $CD16^+$ NK cell in tamarins is very useful tool to understand the relationship between the chimeric virus and $CD16^+$ NK cells. Moreover, it is still unclear whether NK cells might play a pivotal role at the acute or chronic phase in hepatitis. Analyses to address this issue are in progress using our GBV-B model.

Unexpectedly, almost complete *in vivo* depletion of $CD16^+$ NK cells was not able to completely remove the NK activity in PBMCs, i.e., about one-third of the NK activity remained as compared with that before mAb treatment. This indicates that the $CD16^-$ subpopulation represents a substantial component of NK cells in monkeys. So far, mAbs recognizing tamarin's NK-specific CD markers other than CD16, such as CD56 and CD159A (Choi et al., 2008), are not available. Further characterization and phenotyping of NK cells in tamarins will be necessary to selectively and totally deplete NK cells *in vivo*.

Interestingly, tamarins have been used for the study of experimental infection with Rabies virus, Epstein–Barr virus, Hepatitis A virus and Herpesvirus as well as GBV-B (Mackett et al., 1996; Batista-Morais et al., 2000; Purcell et al., 2002; de Thoisy et al., 2003; Martin et al., 2003; Takikawa et al., 2010). Therefore we hope that our system may be useful for examining the role of NK cells in the control of viral infection as well as to develop novel antiviral strategies.

## ACKNOWLEDGMENTS

We would like to give special thanks to Dr. Hiroaki Shibata and members of Corporation for Production and Research of Laboratory Primates for technical assistance. Reagents used in this study were provided by the NIH Non-human Primate Reagent Resource (R24 RR016001, NIAID contract HHSN272200900037C). This work was supported by grants from the Ministry of Health, Labor and Welfare of Japan (to Hirofumi Akari) and Ministry of Education, Culture, Sports, Science and Technology of Japan (to Tomoyuki Yoshida and Hirofumi Akari) and Ministry of the Environment of Japan (to Tomoyuki Yoshida and Hirofumi Akari) and by Global COE Program A06 of Kyoto University.

## REFERENCES

Akari, H., Iwasaki, Y., Yoshida, T., and Iijima, S. (2009). Non-human primate surrogate model of hepatitis C virus infection. *Microbiol. Immunol.* 53, 53–57.

Akari, H., Terao, K., Murayama, Y., Nam, K. H., and Yoshikawa, Y. (1997). Peripheral blood CD4+ CD8+ lymphocytes in cynomolgus monkeys are of resting memory T lineage. *Int. Immunol.* 9, 591–597.

Batista-Morais, N., Neilson-Rolim, B., Matos-Chaves, H. H., de Brito-Neto, J., and Maria-da-Silva, L. (2000). Rabies in tamarins (*Callithrix jacchus*) in the state of Ceara, Brazil, a distinct viral variant? *Mem. Inst. Oswaldo Cruz* 95, 609–610.

Biron, C. A., Byron, K. S., and Sullivan, J. L. (1989). Severe herpesvirus infections in an adolescent without natural killer cells. *N. Engl. J. Med.* 320, 1731–1735.

Bukh, J., Apgar, C. L., and Yanagi, M. (1999). Toward a surrogate model for hepatitis C virus: an infectious molecular clone of the GB virus-B hepatitis agent. *Virology* 262, 470–478.

Cheent, K., and Khakoo, S. I. (2010). Natural killer cells and hepatitis C: action and reaction. *Gut.* doi:10.1136/gut.2010.212555. [Epub ahead of print].

Choi, E. I., Wang, R., Peterson, L., Letvin, N. L., and Reimann, K. A. (2008). Use of an anti-CD16 antibody for in vivo depletion of natural killer cells in rhesus macaques. *Immunology* 124, 215–222.

Cohen, J., and Lester, B. (2007). AIDS research. Trials of NIH's AIDS vaccine get a yellow light. *Science* 318, 1852.

de Thoisy, B., Pouliquen, J. F., Lacoste, V., Gessain, A., and Kazanji, M. (2003). Novel gamma-1 herpesviruses identified in free-ranging new world monkeys (golden-handed tamarin [*Saguinus midas*], squirrel monkey [*Saimiri sciureus*], and white-faced saki [*Pithecia pithecia*]) in French guiana. *J. Virol.* 77, 9099–9105.

Deignan, T., Curry, M. P., Doherty, D. G., Golden-Mason, L., Volkov, Y., Norris, S., Nolan, N., Traynor, O., McEntee, G., Hegarty, J. E., and O'Farrelly, C. (2002). Decrease in hepatic CD56(+) T cells and V alpha 24(+) natural killer T cells in chronic hepatitis C viral infection. *J. Hepatol.* 37, 101–108.

Fleit, H. B., Wright, S. D., and Unkeless, J. C. (1982). Human neutrophil Fc gamma receptor distribution and structure. *Proc. Natl. Acad. Sci. U.S.A.* 79, 3275–3279.

Golden-Mason, L., Madrigal-Estebas, L., McGrath, E., Conroy, M. J., Ryan, E. J., Hegarty, J. E., O'Farrelly, C., and Doherty, D. G. (2008). Altered natural killer cell subset distributions in resolved and persistent hepatitis C virus infection following single source exposure. *Gut* 57, 1121–1128.

Ishii, K., Iijima, S., Kimura, N., Lee, Y. J., Ageyama, N., Yagi, S., Yamaguchi, K., Maki, N., Mori, K., Yoshizaki, S., Machida, S., Suzuki, T., Iwata, N., Sata, T., Terao, K., Miyamura, T., and Akari, H. (2007). GBV-B as a pleiotropic virus: distribution of GBV-B in extrahepatic tissues in vivo. *Microbes Infect.* 9, 515–521.

Kanto, T. (2008). Virus associated innate immunity in liver. *Front. Biosci.* 13, 6183–6192.

Kasai, M., Iwamori, M., Nagai, Y., Okumura, K., and Tada, T. (1980). A glycolipid on the surface of mouse natural killer cells. *Eur. J. Immunol.* 10, 175–180.

Lanford, R. E., Chavez, D., Notvall, L., and Brasky, K. M. (2003). Comparison of tamarins and marmosets as hosts for GBV-B infections and the effect of immunosuppression on duration of viremia. *Virology* 311, 72–80.

Lecoeur, H., Fevrier, M., Garcia, S., Riviere, Y., and Gougeon, M. L. (2001). A novel flow cytometric assay for quantitation and multiparametric characterization of cell-mediated cytotoxicity. *J. Immunol. Methods* 253, 177–187.

Lian, R. H., and Kumar, V. (2002). Murine natural killer cell progenitors and their requirements for development. *Semin. Immunol.* 14, 453–460.

Liu, Z. X., Govindarajan, S., Okamoto, S., and Dennert, G. (2000). NK cells cause liver injury and facilitate the induction of T cell-mediated immunity to a viral liver infection. *J. Immunol.* 164, 6480–6486.

Mackett, M., Cox, C., Pepper, S. D., Lees, J. F., Naylor, B. A., Wedderburn, N., and Arrand, J. R. (1996). Immunisation of common marmosets with vaccinia virus expressing Epstein–Barr virus (EBV) gp340 and challenge with EBV. *J. Med. Virol.* 50, 263–271.

Martin, A., Bodola, F., Sangar, D. V., Goettge, K., Popov, V., Rijnbrand, R., Lanford, R. E., and Lemon, S. M. (2003). Chronic hepatitis associated with GB virus B persistence in a tamarin after intrahepatic inoculation of synthetic viral RNA. *Proc. Natl. Acad. Sci. U.S.A.* 100, 9962–9967.

Navarro-Sánches, E., Desprès, P., and Cedillo-Barrón, L. (2005). Innate immune responses to dengue virus. *Arch. Med. Res.* 36, 425–435.

Orange, J. S. (2002). Human natural killer cell deficiencies and susceptibility to infection. *Microbes Infect.* 4, 1545–1558.

Purcell, R. H., Wong, D. C., and Shapiro, M. (2002). Relative infectivity of hepatitis A virus by the oral and intravenous routes in 2 species of non-human primates. *J. Infect. Dis.* 185, 1668–1671.

Robertson, M. J. (2002). Role of chemokines in the biology of natural killer cells. *J. Leukoc. Biol.* 71, 173–183.

Sbardellati, A., Scarselli, E., Verschoor, E., De Tomassi, A., Lazzaro, D., and Traboni, C. (2001). Generation of infectious and transmissible virions from a GB virus B full-length

consensus clone in tamarins. *J. Gen. Virol.* 82, 2437–2448.

Takikawa, S., Engle, R. E., Faulk, K. N., Emerson, S. U., Purcell, R. H., and Bukh, J. (2010). Molecular evolution of GB virus B hepatitis virus during acute resolving and persistent infections in experimentally infected tamarins. *J. Gen. Virol.* 91, 727–733.

Tenorio, E. P., and Saavedra, R. (2005). Differential effect of sodium arsenite during the activation of human CD4+ and CD8+ T lymphocytes. *Int. Immunopharmacol.* 5, 1853–1869.

Woollard, D. J., Haqshenas, G., Dong, X., Pratt, B. F., Kent, S. J., and Gowans, E. J. (2008). Virus-specific T-cell immunity correlates with control of GB virus B infection in marmosets. *J. Virol.* 82, 3054–3060.

**Conflict of Interest Statement:** The authors declare that the research was conducted in the absence of any commercial or financial relationships that could be construed as a potential conflict of interest.

*Received: 04 August 2010; accepted: 28 October 2010; published online: 08 December 2010.*

*Citation: Yoshida T, Saito A, Iwasaki Y, Iijima S, Kurosawa T, Katakai Y, Yasutomi Y, Reimann KA, Hayakawa T and Akari H (2010) Characterization of natural killer cells in tamarins: a technical basis for studies of innate immunity. Front. Microbio. 1:128. doi: 10.3389/fmicb.2010.00128*

*This article was submitted to Frontiers in Virology, a specialty of Frontiers in Microbiology.*

balt3/zbc-bc/zbc-bc/zbc01711/zbc5609-11z ZSUBMIT 9 xppws S=1 10/2/11 11:08 | 4/Color Figure(s) F3,4,6,7 | ARTNO: M110.185793

THE JOURNAL OF BIOLOGICAL CHEMISTRY VOL. 286, NO. ??, pp. 1–xxx, ???? ??, 2011


# Raftlin Is Involved in the Nucleocapture Complex to Induce Poly(I:C)-mediated TLR3 Activation*[S]

Received for publication, September 15, 2010, and in revised form, January 23, 2011 Published, JBC Papers in Press, January 25, 2011, DOI 10.1074/jbc.M110.185793

**Ayako Watanabe[‡], Megumi Tatematsu[‡], Kazuko Saeki[§], Sachiko Shibata[¶], Hiroaki Shime[‡], Akihiko Yoshimura[‖], Chikashi Obuse[¶], Tsukasa Seya[‡], and Misako Matsumoto[‡1]**

*From the [‡]Department of Microbiology and Immunology, Hokkaido University Graduate School of Medicine, Kita 15, Nishi 7, Kita-ku, Sapporo 060-8638, the [§]Department of Medical Biochemistry, Graduate School of Medical Sciences, Kyushu University, Fukuoka 812-8582, the [¶]Division of Molecular Life Science, Graduate School of Life Science, Hokkaido University, Sapporo 001-0021, and the [‖]Department of Microbiology and Immunology, School of Medicine, Keio University, Tokyo 160-8582, Japan*

**The double-stranded RNA analog, poly(I:C), extracellularly activates both the endosomal Toll-like receptor (TLR) 3 and the cytoplasmic RNA helicase, melanoma differentiation-associated gene 5, leading to the production of type I interferons (IFNs) and inflammatory cytokines. The mechanism by which extracellular poly(I:C) is delivered to TLR3-positive organelles and the cytoplasm remains to be elucidated. Here, we show that the cytoplasmic lipid raft protein, Raftlin, is essential for poly(I:C) cellular uptake in human myeloid dendritic cells and epithelial cells. When Raftlin was silenced, poly(I:C) failed to enter cells and induction of IFN-β production was inhibited. In addition, cellular uptake of B-type oligodeoxynucleotide that shares its uptake receptor with poly(I:C) was suppressed in Raftlin knockdown cells. Upon poly(I:C) stimulation, Raftlin was translocated from the cytoplasm to the plasma membrane where it colocalized with poly(I:C), and thereafter moved to TLR3-positive endosomes. Thus, Raftlin cooperates with the uptake receptor to mediate cell entry of poly(I:C), which is critical for activation of TLR3.**

AQ: A

Fn2 Polyriboinosinic:polyribocytidylic acid (poly(I:C)),[2] a synthetic double-stranded RNA (dsRNA), has been used as a potent type I interferon (IFN-α/β) inducer in both *in vitro* and *in vivo* studies since the discovery of anti-viral activity of type I IFNs (1–3). Many types of cells including fibroblasts, epithelial cells, and myeloid dendritic cells (DCs), produce IFN-β upon stimulation with poly(I:C). Studies have demonstrated that extracellular poly(I:C) is recognized by Toll-like receptor (TLR) 3 and cytoplasmic RNA helicase, melanoma differentiation-associated gene 5 (MDA5), and induces innate immune responses including the production of type I IFNs and inflammatory cytokines (4–8). More recently, experimental evidence has accumulated that poly(I:C) acts as an adjuvant that enhances antibody production, natural killer cell activation, and cytotoxic T lymphocyte induction through the activation of TLR3 and/or MDA5 (9–15).

Human TLR3 localizes to the endosomal compartments in myeloid DCs, whereas it localizes to both the cell surface and endosomes of fibroblasts, macrophages, and epithelial cells (5, 16, 17). TLR3 signaling arises from an intracellular compartment in both cell types and requires endosomal maturation. After dsRNA recognition, endosomal TLR3 recruits an adaptor molecule, *i.e.* Toll-IL-1 receptor domain-containing adaptor molecule-1 (TICAM-1, also called TRIF) that activates the NF-κB, IRF-3, and AP-1 transcription factors, leading to IFN-β production (18, 19). Also, extracellular poly(I:C) is sensed by MDA5 in the cytoplasm, resulting in the activation of IRF-3 and NF-κB via the mitochondrial outer membrane protein IPS-1 (also called MAVS, Cardif, or VISA) (20–23). However, the mechanism by which poly(I:C) is delivered from the extracellular fluid to the intracellular dsRNA sensors remains unresolved.

AQ: B

A recent study showed that CD14 directly binds to poly(I:C) and mediates poly(I:C) cellular uptake (24). Bone marrow-derived macrophages from CD14-deficient mice exhibited impaired, but not completely diminished, responses to poly(I:C). Also, a class A scavenger receptor was identified as a cell surface receptor for poly(I:C) in human epithelial cells, although the response of poly(I:C) was only partially impaired in scavenger receptor A-deficient mice (25). These results suggest that an unidentified cell surface molecule mediates cell entry of poly(I:C). Indeed, we and others demonstrated that poly(I:C) is internalized into CD14-negative human myeloid DCs and HEK293 cells via clathrin-dependent endocytosis, and B- and C-type oligodeoxynucleotides (ODNs) share the uptake receptor with poly(I:C) (26–28).

In this study, we isolated poly(I:C)-binding proteins from CD14-negative cell lysates by sequential affinity chromatography with poly(U)- and poly(I:C)-Sepharose and subjected them to mass spectrometric analysis. Among the proteins identified, we selected several proteins that exhibited a transmembrane domain or a membrane-anchoring motif and examined whether they were involved in poly(I:C)-induced TLR3-mediated signaling. We found that Raftlin, a major lipid raft protein

* This work was supported in part by Grants-in-aid from the Ministry of Education, Science, and Culture, the Ministry of Health, Labor, and Welfare of Japan, and the Akiyama Foundation, NorthTec Foundation, Yakult Foundation, and the Program of Founding Research Centers for Emerging and Reemerging Infectious Diseases, MEXT.

[S] The on-line version of this article (available at http://www.jbc.org) contains supplemental Tables S1–S3 and Figs. S1–S4. ZSI

[1] To whom correspondence should be addressed. Tel.: 81-11-706-6056; Fax: 81-11-706-7866; E-mail: matumoto@pop.med.hokudai.ac.jp.

[2] The abbreviations used are: poly(I:C), polyriboinosinic:polyribocytidylic acid; 4F2, 4F2 cell-surface antigen heavy chain; DCs, dendritic cells; BMDC, bone marrow-derived DC; CTXB, cholera toxin subunit B; MDA5, melanoma differentiation-associated gene 5; MβCD, methyl-β-cyclodextrin; MoDC, monocyte-derived immature DC; ODN, oligodeoxynucleotide; TICAM-1, Toll-IL-1 receptor-containing adaptor molecule-1; TLR, Toll-like receptor.

balt3/zbc-bc/zbc01711/zbc5609-11z ZSUBMIT 9 xppws S=1 10/2/11 11:08 | 4/Color Figure(s) F3,4,6,7 | ARTNO: M110.185793



expressed by B cells, plays a critical role in poly(I:C) cellular uptake in human myeloid DCs and epithelial cells.

## EXPERIMENTAL PROCEDURES

*Cell Culture and Reagents*—Human B cell lines Raji, BALL-1, and Namalwa were obtained from the Riken Cell Bank (Tukuba, Japan) and maintained in RPMI 1640 supplemented with 10% heat-inactivated FCS (BioSource Intl., Inc.) and antibiotics. HEK293 cells were obtained from Sumitomo Pharmaceuticals Co., Ltd. (Osaka, Japan) and maintained in Dulbecco's modified Eagle's medium low glucose (Invitrogen) supplemented with 10% heat-inactivated FCS and antibiotics. HeLa cells were kindly provided by Dr. T. Fujita (Kyoto University) and maintained in Eagle's minimal essential medium (Nissui, Tokyo, Japan) supplemented with 1% L-glutamine and 10% heat-inactivated FCS. Human monocyte-derived immature DCs (MoDCs) were generated from $CD14^+$ monocytes by culturing for 6 days in the presence of 500 units/ml of granulocyte-macrophage colony-stimulating factor and 100 units/ml of IL-4 (PeproTech). Bone marrow-derived DCs (BMDCs) were prepared as described (10). Polymyxin B, 4′,6-diamidine-2′-phenylindole dihydrochloride (DAPI), saponin, and methyl-β-cyclodextrin (MβCD) were purchased from Sigma. Poly(I:C) was from Amersham Biosciences, FITC-labeled ODN2006 was from InvivoGen, Alexa Fluor 488/cholera toxin subunit B (CTXB) and Alexa Fluor 568/transferrin were from Molecular Probes. MALP-2 was obtained from Biosynthesis (Nagoya, Japan). In addition, the following antibodies were used in this study: anti-dsRNA mAb (K1) (BioLink), anti-β actin mAb (Sigma), anti-clathrin heavy chain mAb (TD.1) (Santa Cruz Biotechnology), anti-Rab5 mAb (Abcam), anti-LAMP1 (H4A3) (BioLegend), HRP-conjugated secondary Abs (BIOSOURCE), FITC-labeled goat anti-mouse IgG (American Qualex), and Alexa Fluorp®-conjugated secondary antibodies (Invitrogen). Anti-human Raftlin polyclonal antibody was prepared as described (29). Anti-human TLR3 mAb (clone TLR3.7) was generated in our laboratory (5). Texas Red-labeled poly(I:C) was prepared using the 5′ EndTag™ Nucleic Acid Labeling System (Vector Laboratories, Burlingame, CA) according to the manufacturer's instructions.

*Mice*—Raftlin$^{-/-}$ mice were provided by Dr. A. Yoshimura (Keio University). Mice were maintained under specific pathogen-free conditions in the animal facility of the Hokkaido University Graduate School of Medicine. Animal experiments were performed according to the guidelines established by the Hokkaido University Animal Care and Use Committee.

*Plasmids*—The cDNA fragment encoding the ORF of human TLR2 or TLR3 was amplified by RT-PCR from total RNA prepared from MoDCs, and was ligated into the cloning site of the expression vector pEF-BOS, a gift from Dr. S. Nagata (Kyoto University) (5). Complementary DNA for human Raftlin was generated by PCR from cDNA derived from Raji cells using specific primers (forward primer, 5′-CTCGAGGCCGCCACCATGGGTTG-3′; reverse primer, 5′-GGATCCTTGTTTTCTTCAACCGTACCAAGCTC-3′), and was ligated into the cloning site of the expression vector pEYFP-N1 (C-terminal yellow fluorescent protein (YFP) tag, Clontech).

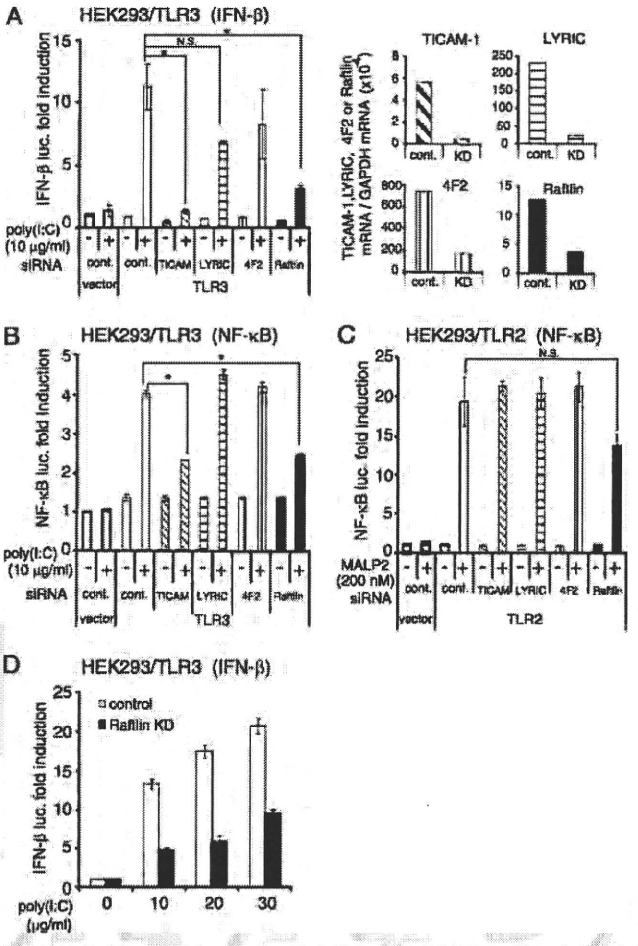


FIGURE 1. **Raftlin participates in poly(I:C)-induced TLR3-mediated signaling.** HEK293 cells were transfected with the indicated siRNAs (20 pmol) together with the expression vector for human TLR3 (*A*, *B*, and *D*), human TLR2 (*C*), or empty vector and reporter plasmid. Forty-eight hours after transfection, cells were washed and stimulated with 10–30 μg/ml of poly(I:C) or 200 nM MALP-2. After 6 h, the luciferase reporter activities were measured and expressed as fold-induction relative to the activity of unstimulated vector-transfected cells. Representative data from a minimum of three separate experiments are shown (mean ± S.D.). In each experiment, knockdown (*KD*) efficiency was assessed 48 h after transfection by qPCR. Expression of each gene was normalized to GAPDH mRNA expression. As shown in the *right-hand panels* of *A*, expression of the indicated genes is efficiently silenced (knockdown efficiency: TICAM-1, 91.4%; LYRIC, 89.5%; 4F2, 77.4%; Raftlin, 71.8%). *, $p < 0.05$ (*t* test).

*Isolation of Poly(I:C)-binding Proteins*—Raji cells ($1 \times 10^{10}$) were washed twice with Dulbecco's phosphate-buffered saline, frozen and thawed three times in Dulbecco's phosphate-buffered saline ($5 \times 10^7$/ml), and centrifuged at 20,000 × *g* for 10 min. Cell pellets were lysed in lysis buffer (1% Nonidet P-40 in buffer A (20 mM Tris-HCl, pH 7.4, 140 mM NaCl, 25 mM IAA, 10 mM EDTA, 2 mM PMSF and protease inhibitor mixture)) for 20 min at room temperature. After centrifugation at 10,000 × *g* for 10 min, supernatants were filtrated with Minisalt GF (Zartorius stedim, Japan) and sequentially applied to Sepharose, poly(U)-Sepharose, and poly(I:C)-Sepharose equilibrated with binding buffer (0.2% Nonidet P-40 in buffer A). The poly(I:C)-binding molecules were eluted from poly(I:C)-Sepharose with elution buffer (1.4 M NaCl in washing buffer) after being washed with washing buffer (10 mM CHAPS in buffer A). The eluates were

balt3/zbc-bc/zbc-bc/zbc01711/zbc5609-11z ZSUBMIT 9 xppws S=1 10/2/11 11:08 | 4/Color Figure(s) F3,4,6,7 | ARTNO: M110.185793



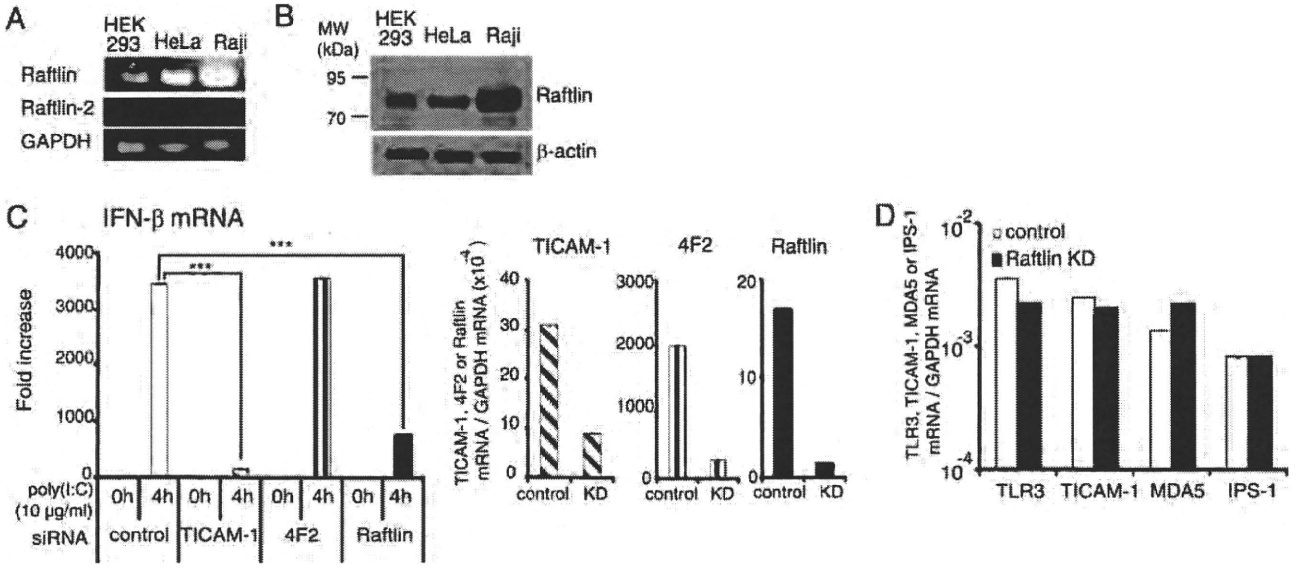


FIGURE 2. **Raftlin is essential for poly(I:C)-induced IFN-β production in HeLa cells.** *A*, expression of Raftlin and Raftlin-2 mRNAs in human cell lines. *B*, protein expression level of Raftlin in human cell lines. Cell lysates (3 μg) were separated on 10% SDS-PAGE, followed by immunoblotting with anti-Raftlin pAb or anti-β-actin mAb. *C*, poly(I:C)-induced IFN-β mRNA expression in HeLa cells. HeLa cells were transfected with the indicated siRNAs (20 pmol) using Lipofectamine 2000. Forty-eight hours after transfection, cells were washed and stimulated with 10 μg/ml of poly(I:C) for 4 h (*left-hand panel*). Total RNA was extracted and qPCR was performed using primers for the respective genes (*C* and *D*). Expression of each gene was normalized to GAPDH mRNA expression. Data are shown as the mean ± S.D., although the values are too small to represent. Representative data from three independent experiments are shown. ***, $p < 0.001$.

mixed with new poly(U)-Sepharose and rotated for 1 h at 4 °C. After centrifugation, supernatants were mixed with new poly(I:C)-Sepharose. The poly(U)- and poly(I:C)-Sepharose were washed three times with 5 volumes of washing buffer and binding molecules were eluted with elution buffer. The eluates were concentrated using YM-50 Microcon (Millipore).

*Mass Spectrometry*—The poly(U)- or poly(I:C)-binding molecules were separated on a 10% SDS-PAGE gel under reducing conditions, and the region of the gels containing proteins from about 250,000 to 20,000 was cut at about 1–2-mm intervals as described previously (30). After in-gel digestion with modified trypsin, the resulting peptides were analyzed by LC/MS/MS. The ion spectrum data generated by LC/MS/MS were screened against the international protein index human data base (version 3.29) with Mascot (Matrix Science, London, UK) to identify high-scoring proteins.

*RNA Interference and Luciferase Reporter Assay*—siRNA duplexes (LYRIC, catalog number s40866; 4F2, catalog number s12944; Raftlin, catalog numbers s23219, s23217, and s23218; negative control, catalog number AM4635) were obtained from Ambion-Applied Biosystems. siRNA for TICAM-1 was purchased from Xeragon Inc. (Birmingham, AL) (18). HEK293 cells cultured in 24-well plates were transfected with 20 pmol of each siRNA together with the expression vector for human TLR3 or TLR2 (200 ng), IFN-β promoter or ELAM reporter plasmid (60 ng), and an internal control vector (1.5 ng) using Lipofectamine 2000. Forty-eight hours after transfection, cells were washed once and then stimulated with 10 μg/ml of poly(I:C) or MALP-2 (200 nM) for 6 h. Cells were lysed and dual luciferase activities were measured according to the manufacturer's instructions (Promega). The *Firefly* luciferase activity was normalized to the *Renilla* activity and expressed as the fold-induction relative to the activity of unstimulated vector-transfected cells. In the case of HeLa cells, cells in 24-well plates were transfected with 20 pmol of each siRNA using Lipofectamine 2000. Knockdown of Raftlin in human MoDCs was preformed by electroporation as described previously (31). Briefly, MoDCs ($1.4 \times 10^6$/80 μl) were transfected with control siRNA or siRNA for Raftlin (500 pmol) using a Gene-Pulser (Bio-Rad) and then cultured for 36 h in the presence of 500 milliunits/ml of granulocyte-macrophage colony-stimulating factor. The viability of the cells transfected with control and Raftlin siRNAs was 84 and 87%, respectively. Knockdown of mouse Raftlin-2 in Raftlin$^{-/-}$ BMDCs was performed with shRNA lentiviral particles (Santa Cruz) according to the manufacturer's instructions. Briefly, Raftlin$^{-/-}$ BMDCs in 24-well plates were infected with control shRNA lentiviral particles or mouse Raftlin-2 shRNA lentiviral particles at a multiplicity of infection of 2 and incubated in complete medium containing Polybrene (5 μg/ml). Twenty-four hours after infection, medium was replaced with complete medium and cells were further incubated for 24 h. The viability of the cells infected with control lentivirus and mouse Raftlin-2 shRNA-expressing lentivirus was 82 and 76%, respectively.

*Quantitative PCR (qPCR)*—Total RNA was extracted with the RNeasy mini kit (Qiagen, Valencia, CA) and 0.5 μg of RNA was reverse-transcribed using the high capacity cDNA Reverse Transcripition kit (Applied Biosystems) with random primers according to the manufacturer's instructions. Quantitative PCR was performed with the indicated primers (supplemental Table S1) using the Step One Real-time PCR system (Applied Biosystems).

*Immunoblotting*—Cells were lysed in lysis buffer (20 mM Tris-HCl, pH 7.4) containing 150 mM NaCl, 1% Nonidet P-40,

balt3/zbc-bc/zbc-bc/zbc01711/zbc5609-11z ZSUBMIT 9 xppws S=1 10/2/11 11:08 | 4/Color Figure(s) F3,4,6,7 | ARTNO: M110.185793



10 mM EDTA, 25 mM iodoacetamide, 2 mM PMSF and a protease inhibitor mixture (Roche Applied Science). Lysates were clarified by centrifugation and subjected to SDS-PAGE (10% gel) under reducing conditions, followed by immunoblotting with anti-Raftlin pAb or anti-$\beta$ actin mAb.

*Immunoprecipitation*—HeLa cells were stimulated with 40 $\mu$g/ml of poly(I:C) for 30 min at 37 °C. At timed intervals, cells were lysed in lysis buffer for 30 min on ice. Lysates were precleared with protein G-Sepharose (GE Healthcare) and incubated with 1 $\mu$g of anti-clathrin heavy chain mAb. Immunocomplexes were recovered by incubation with Protein G-Sepharose, washed once with lysis buffer, and resuspended in denaturing buffer. Samples were analyzed by SDS-PAGE (10% gel) under reducing conditions, followed by immunoblotting with anti-Raftlin pAb (1:1000) and HRP-conjugated secondary Ab. The membrane was re-probed with anti-clathrin heavy chain mAb (1:400).

*Confocal Microscopy*—HeLa cells ($1 \times 10^5$ cells/well) were plated onto micro coverglasses (Matsunami Glass) in 12-well plates. The next day, cells were incubated with 40 $\mu$g/ml of poly(I:C) for 30 min at 4 °C. Cells were washed once and further incubated for 5–30 min at 37 °C. At timed intervals, cells were fixed with 4% paraformaldehyde for 30 min and permeabilized with PBS containing 0.5% saponin and 1% BSA for 30 min. Fixed cells were blocked in PBS containing 1% BSA and labeled with anti-Raftlin pAb (1:500), anti-human TLR3 mAb (20 $\mu$g/ml), or Alexa Fluor 488-CTXB (10 $\mu$g/ml) for 60 min at room temperature. Alexa Fluor 488- or Alexa Fluor 568-conjugated secondary Abs (1:400) were used to visualize the primary Abs. Nuclei were stained with DAPI (2 $\mu$g/ml) in PBS for 10 min before mounting onto glass slides using PBS containing 2.3% DABCO and 50% glycerol. Cells were visualized at a ×63 magnification with an LSM510 META microscope (Zeiss, Jena, Germany).

For uptake study, HeLa cells or HEK293 cells transfected with control siRNA or siRNA for Raftlin were incubated with 40 $\mu$g/ml of Texas Red/poly(I:C), Alexa Fluor 568/transferrin (25 $\mu$g/ml), or FITC/ODN2006 (40 $\mu$g/ml) for 30 min at 4 °C. After washing, cells were further incubated at 37 °C. At timed intervals, fixed cells were visualized as described above. In the case of HEK293 cells, cells ($1 \times 10^5$ cells/well) were plated onto poly-L-lysine-coated glass (BD Bioscience) in a 24-well plate and cultured for 12 h.

Control or Raftlin knockdown MoDCs ($2 \times 10^5$/100 $\mu$l) were incubated with 40 $\mu$g/ml of Texas Red/poly(I:C) for 30 min at 4 °C, washed once, and then incubated for 5–30 min at 37 °C. At timed intervals, cells were fixed with 4% paraformaldehyde for 15 min and centrifuged by Cytospin3 (Shandon). After mounting with ProLong Gold with DAPI (Molecular Probes), cells were visualized by confocal microscopy. In some experiments, MoDCs were pretreated with 1 mM M$\beta$CD for 1 h at 37 °C. Viability of cells treated with M$\beta$CD was 93.3%. For staining of endosomes, fixed cells were permeabilized with PBS containing 0.5% saponin and 1% BSA for 30 min (staining of TLR3 and early endosome), or PBS containing 100 $\mu$g/ml of digitonin and 1% BSA for 30 min (staining of late endosome). After blocking, cells were labeled with anti-Raftlin pAb (1:500), anti-human TLR3 mAb (20 $\mu$g/ml), anti-Rab5 mAb (4 $\mu$g/ml), or anti-LAMP1 mAb (H4A3) (1:200) for 60 min at room temperature.

*Flow Cytometry*—Cells were incubated with the indicated concentrations of poly(I:C) in culture medium for 30 min at 4 °C. After washing, cells were labeled with anti-dsRNA mAb

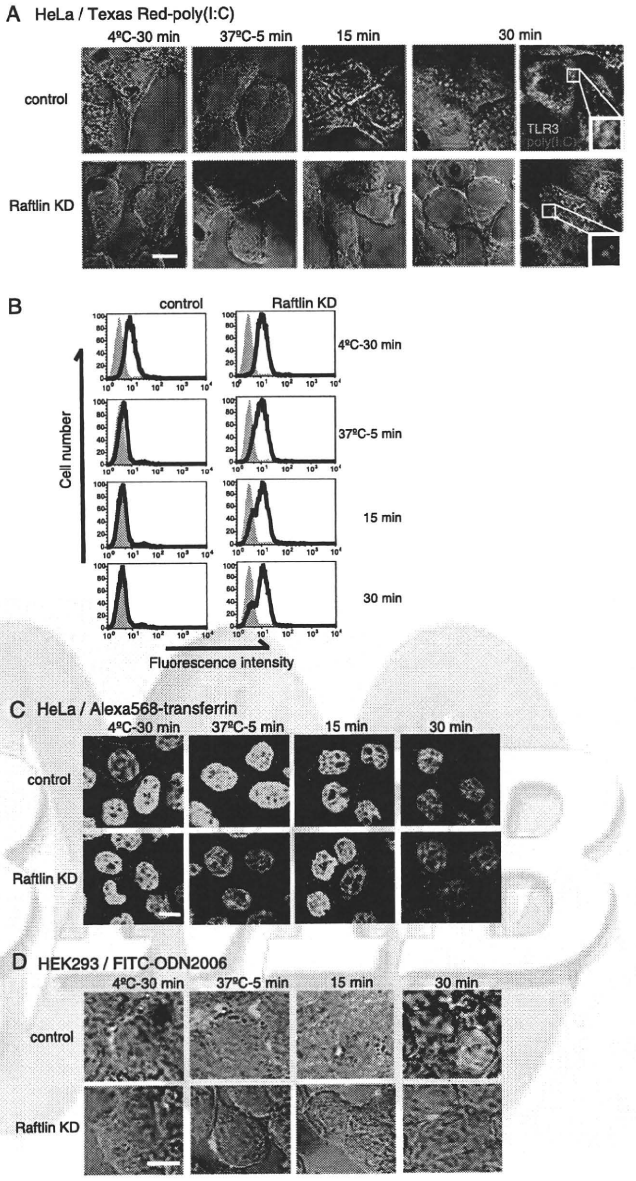


FIGURE 3. **Knockdown of Raftlin suppresses cellular uptake of poly(I:C) and B-type ODN but not transferrin.** HeLa cells (*A* and *C*) and HEK293 cells (*D*) were transfected with control siRNA (*upper panels*) or siRNA for Raftlin (*lower panels*). Forty-eight hours after transfection, cells were washed and incubated with 40 $\mu$g/ml of Texas Red/poly(I:C) (*A*), 25 $\mu$g/ml Alexa Fluor 568/transferrin (*C*), or 40 $\mu$g/ml of FITC/ODN2006 (*D*) for 30 min at 4 °C. After washing, cells were incubated for up to 30 min at 37 °C. At timed intervals, cells were fixed and visualized by confocal microscopy. In some experiments, cells were fixed or permeabilized and stained with anti-TLR3 mAb. *A*, *red*, Texas Red-poly(I:C); *green*, TLR3. *C*, *red*, Alexa 568/transferrin; *blue*, nuclei with DAPI. *D*, *green*, FITC/ODN2006. *Bar*, 10 $\mu$m. *B*, flow cytometric analysis of poly(I:C) uptake. Control and Raftlin knockdown HeLa cells were incubated with 20 $\mu$g/ml of poly(I:C) for 30 min at 4 °C. After washing, cells were incubated for up to 30 min at 37 °C. At the indicated time points, cells were labeled with anti-dsRNA mAb (*black lines*) or mouse IgG2a (*shaded histogram*) and FITC-labeled secondary Ab. The cells were analyzed on a FACS Calibur.

balt3/zbc-bc/zbc-bc/zbc01711/zbc5609-11z ZSUBMIT 9 xppws S=1 10/2/11 11:08 | 4/Color Figure(s) F3,4,6,7 | ARTNO: M110.185793



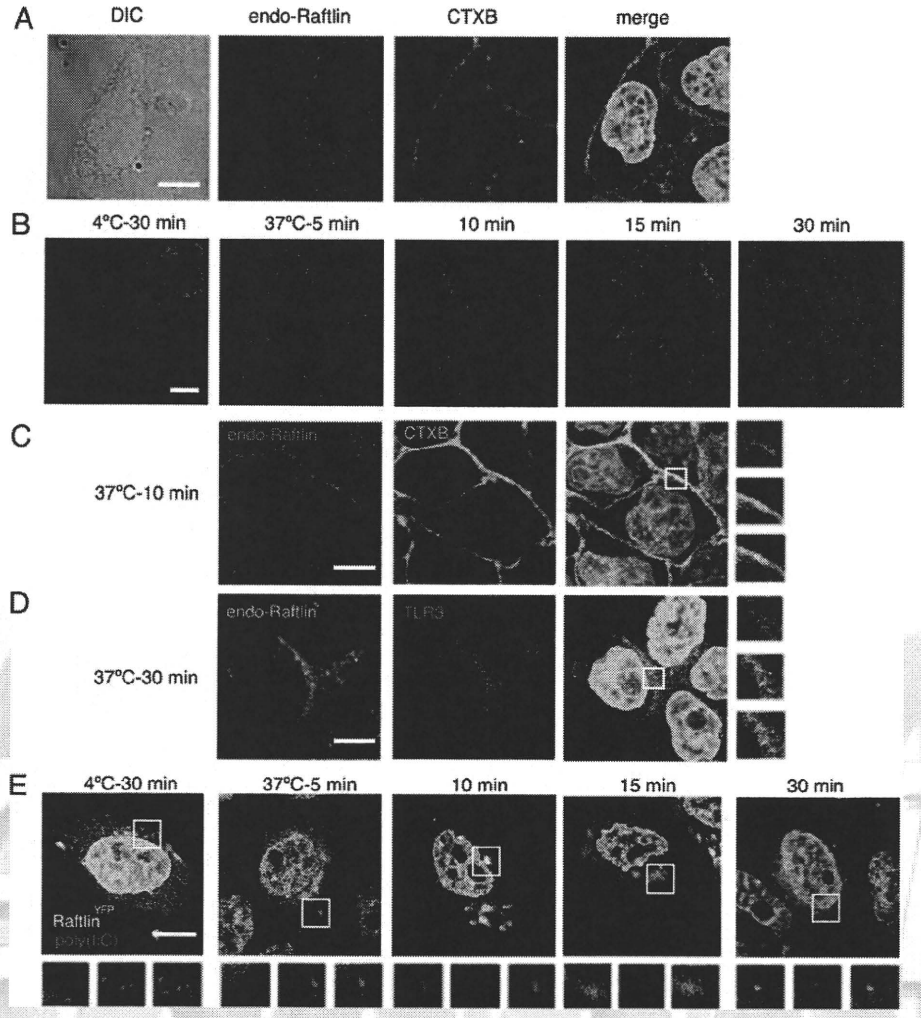


COLOR

FIGURE 4. **Translocation of Raftlin in response to poly(I:C).** *A*, confocal images of endogenous Raftlin in HeLa cells. Fixed and permeabilized cells were stained with anti-Raftlin pAb and Alexa Fluor 488/CTXB. *Red*, endogenous Raftlin; *green*, CTXB; *blue*, nuclei with DAPI. *Bar*, 10 $\mu$m. *B–D*, spatiotemporal mobilization of endogenous Raftlin in response to poly(I:C). HeLa cells were incubated with 40 $\mu$g/ml of poly(I:C) as described in the legend to Fig. 3. At the indicated periods, cells were fixed and stained with anti-Raftlin pAb (*B*), anti-Raftlin pAb and Alexa Fluor 488/CTXB (*C*), or anti-Raftlin pAb and anti-TLR3 mAb (*D*). Representative data from the indicated time points are shown. *B* and *C*, *red*, endogenous Raftlin; *green*, Alexa 488/CTXB. *D*, *green*, endogenous Raftlin; red, TLR3; *blue*, nuclei with DAPI. *Bar*, 10 $\mu$m. *E*, association of Raftlin with poly(I:C). Confocal images of poly(I:C) uptake by HeLa cells expressing Raftlin$^{YFP}$. HeLa cells were transfected with Raftlin$^{YFP}$ and incubated with 40 $\mu$g/ml of Texas Red/poly(I:C) as described above. At the indicated periods, cells were fixed and visualized by confocal microscopy. *Lower panels* show ×2 magnified images of the *insets* in the *upper panels*. *Yellow*, Raftlin$^{YFP}$; *red*, Texas Red/poly(I:C); *blue*, nuclei with DAPI. *Bar*, 10 $\mu$m.

(K1) or mouse IgG2a as a control (1 $\mu$g) in the presence of human IgG (10 $\mu$g) for 30 min at 4 °C in FACS buffer (Dulbecco's phosphate-buffered saline containing 0.5% BSA and 0.1% sodium azide) and then incubated with FITC-labeled secondary Ab. Cells were analyzed on a FACS Calibur flow cytometer (BD Biosciences).

*Statistical Analysis*—Statistical significance of differences between groups was determined by the Student's *t* test.

## RESULTS

*Raftlin Participates in Poly(I:C)-induced TLR3-mediated Signaling*—We previously demonstrated that poly(I:C) binds to human MoDCs and HEK293 cells (27). Because poly(I:C) also activates B cells (32), we screened B cell lines capable of binding poly(I:C) and found that Raji cells bound poly(I:C) at an equivalent level to MoDCs (supplemental Fig. S1). To identify the proteins involved in poly(I:C) cellular uptake, we isolated the poly(I:C)-binding proteins from Raji cell lysates by sequential affinity chromatography using Sepharose, poly(U)-Sepharose, and poly(I:C)-Sepharose. The eluate from poly(U)- or poly(I:C)-Sepharose was subjected to SDS-PAGE, followed by mass spectrometric analyses. A total of 127 proteins were identified, which preferentially bound to poly(I:C)-Sepharose rather than to poly(U)-Sepharose (supplemental Table S2). They included several proteins with a dsRNA-binding motif, such as interferon-induced dsRNA-activated protein kinase (supplemental Table 3). Also, clathrin heavy chain 1 and several cytoskeleton molecules, such as tubulin and actinin-1, were identified, suggesting that poly(I:C) uptake machinery might be isolated from the cell lysates as a complex. In the membrane/cytoskeleton group, only four are membrane-associated proteins (supplemental Table S3). We selected transmembrane proteins LYRIC

AQ: G

ZSI

(also called Astrocyte elevated gene 1) and 4F2 cell surface antigen heavy chain (4F2, also named CD98), and a cytoplasmic protein Raftlin that contains a membrane-anchoring motif at the N terminus. Because HEK293 cells express these molecules, we first examined whether they are involved in poly(I:C)-induced TLR3-mediated signaling by gene silencing. As a positive control, knockdown of TICAM-1 was performed. Interestingly, poly(I:C)-induced TLR3-mediated IFN-β promoter activation was greatly reduced when Raftlin was knocked down in HEK293 cells, whereas silencing of the LYRIC or 4F2 genes did not affect poly(I:C) function (Fig. 1*A*, *left-hand panel*). Poly(I:C)-induced TLR3-mediated NF-κB activation was also decreased in Raftlin knockdown HEK293 cells, in a similar way to TICAM-1 knockdown cells (Fig. 1*B*). In contrast, TLR2-mediated NF-κB activation was substantially induced in all cells subjected to gene silencing (Fig. 1*C*). The failure of IFN-β promoter activation in Raftlin knockdown HEK293 cells was also observed when cells were stimulated with increasing amounts of poly(I:C) (Fig. 1*D*). These results strongly suggest that Raftlin participates in poly(I:C)-induced TLR3 activation.

*Raftlin Is Essential for Poly(I:C)-induced IFN-β Production in HeLa Cells*—Raftlin was originally identified as a major lipid raft protein required for lipid raft integrity, B cell receptor signal transduction, and modulation of T cell receptor signaling (29, 33). We analyzed the expression of Raftlin and Raftlin-2, a homologue of Raftlin, in HEK293, HeLa, and Raji cells by RT-PCR. As shown in Fig. 2*A*, these cell lines express Raftlin but not Raftlin-2 mRNA. The protein expression level of Raftlin was further examined by immunoblotting with an anti-human Raftlin pAb (29). Raftlin was abundantly expressed in Raji cells, and expressed at lower levels in HEK293 and HeLa cells (Fig. 2*B*). Poly(I:C)-induced IFN-β mRNA expression was greatly diminished by knockdown of Raftlin in HeLa cells, in a similar way to TICAM-1 knockdown. In contrast, HeLa cells transfected with siRNA for 4F2 or LYRIC efficiently responded to poly(I:C) (Fig. 2*C*, *left-hand panel*, and supplemental Fig. S2). The expression of TLR3, TICAM-1, MDA5, and IPS-1 was not affected by knockdown of Raftlin (Fig. 2*D*). Thus, Raftlin plays a critical role in poly(I:C)-induced IFN-β production.

*Raftlin Is Indispensable for Poly(I:C) Cellular Uptake*—To examine the role of Raftlin in poly(I:C)-induced cellular responses, we analyzed cell entry of poly(I:C) in Raftlin knockdown HeLa cells. Texas Red-labeled poly(I:C), whose biological activity was similar to that of unlabeled poly(I:C) (supplemental Fig. S3), unevenly bound to the cell surface of HeLa cells either transfected with control siRNA or Raftlin siRNA after 30 min incubation at 4 °C (Fig. 3*A*, *left panels*). When the incubation condition was changed to 37 °C for 5 min, poly(I:C) was detected as speckles at the cell surface in both cells, although some of the poly(I:C) was internalized in control cells (*second set of panels*). However, after 15 min, poly(I:C) localized diffusely in the endosomal compartments in control cells, whereas it still resided on the cell surface as speckles in Raftlin knockdown cells (*third set of panels*). Thus, clustering of the uptake receptor occurs without internalization in Raftlin knockdown cells. After 30 min, poly(I:C) accumulated in the endosomal compartments in control cells, where it colocalized with TLR3 (Fig. 3*A*, *upper right panel*). In contrast, Raftlin knockdown

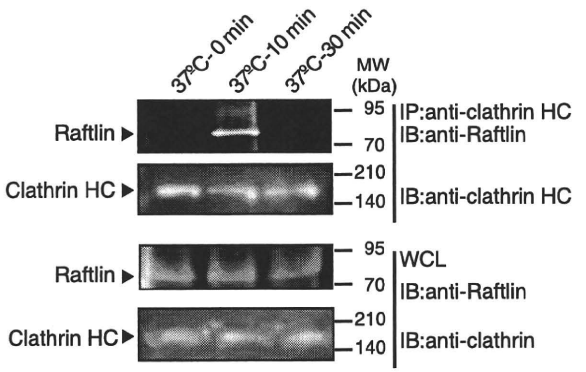


FIGURE 5. **Raftlin associates with clathrin in response to poly(I:C).** HeLa cells were stimulated with 40 μg/ml of poly(I:C) for 0–30 min at 37 °C. At timed intervals, cells were lysed in lysis buffer and clathrin was immunoprecipitated (*IP*) using an anti-clathrin heavy chain (*HC*) mAb. The immunoprecipitants were resolved on SDS-PAGE (10% gel) under reducing conditions followed by immunoblotting (*IB*) with anti-Raftlin pAb or anti-clathrin HC mAb. Whole cell lysates (*WCL*) were subjected to immunoblotting with anti-Raftlin pAb or anti-clathrin HC mAb to detect endogenous protein expression. Molecular mass markers are indicated on the *right*.

HeLa cells did not permit cell entry of poly(I:C). Consistent with these results, flow cytometric analysis showed that surface poly(I:C) disappeared in control but not in Raftlin knockdown HeLa cells (Fig. 3*B*). After a 30-min incubation at 37 °C, poly(I:C) was detected on the cell surface of ~80% of HeLa cells transfected with Raftlin-siRNA, which reflects the knockdown efficiency.

Because poly(I:C) is internalized into cells by the clathrin-dependent endocytic pathway, we examined whether uptake of transferrin, which occurs in a clathrin-dependent manner, is suppressed by Raftlin knockdown. As shown in Fig. 3*C*, transferrin was internalized into HeLa cells irrespective of Raftlin knockdown. We previously reported that B- and C-type ODNs share their uptake receptor with poly(I:C) in HEK293 cells and MoDCs and are delivered to TLR3-positive endosomes in MoDCs (27). Indeed, FITC-labeled B-type ODN (ODN 2006) failed to enter cells when Raftlin was silenced in HEK293 cells (Fig. 3*D*). These results indicate that Raftlin is essential for uptake of poly(I:C) and B- and C-type ODNs via receptor-mediated endocytosis.

*Raftlin Is Involved in the Uptake Machinery for Poly(I:C)*—A previous study showed that Raftlin is localized exclusively in lipid rafts by fatty acylation of the N-terminal Gly-2 and Cys-3 residues in human B cells (29). We analyzed the subcellular localization of Raftlin in HeLa cells. Endogenous Raftlin was localized diffusely in the cytoplasm and did not merge with CTXB, which binds to the lipid raft molecule GM1, suggesting the cell type-dependent localization of Raftlin (Fig. 4*A*). We next examined the translocation of Raftlin in response to poly(I:C). At the poly(I:C) binding step (4 °C, 30 min), Raftlin resided in the cytoplasm (Fig. 4*B*, *left panel*). After a 5-min incubation at 37 °C, most of the Raftlin remained localized in the cytoplasm. However, after 10 min, membrane-associated Raftlin was observed, which partially colocalized with CTXB (Fig. 4, *B*, *third panel*, and *C*). Interestingly, Raftlin transferred to the endosomal structures from the plasma membrane within 15 min, and colocalized with TLR3 after 30 min of incubation (Fig. 4*D*).

balt3/zbc-bc/zbc-bc/zbc01711/zbc5609-11z ZSUBMIT 9 xppws S=1 10/2/11 11:08 | 4/Color Figure(s) F3,4,6,7 | ARTNO: M110.185793



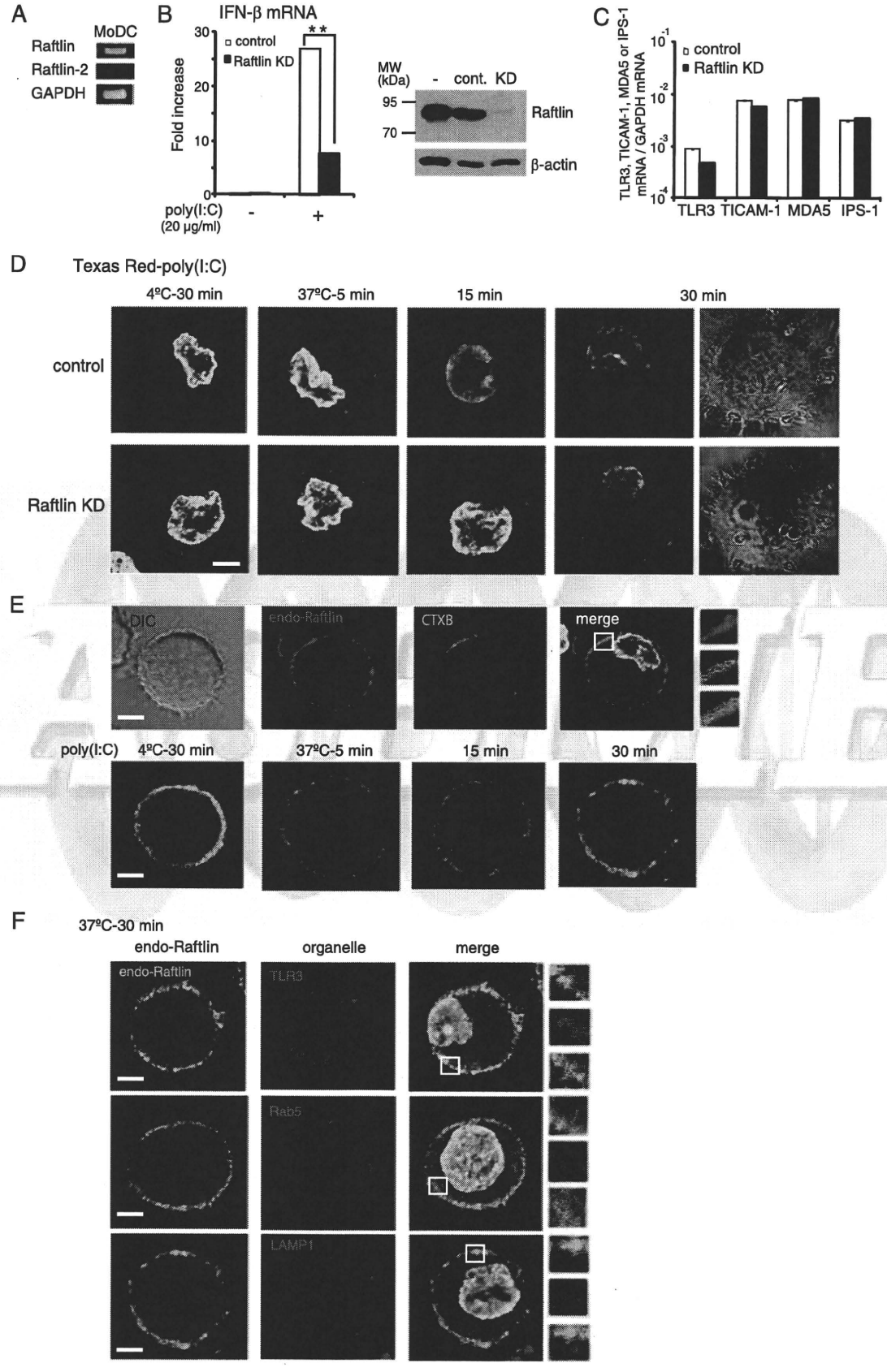

## Essential Role of Raftlin in Poly(I:C) Cellular Uptake

To visualize the spatiotemporal mobilization of Raftlin and poly(I:C), HeLa cells were transfected with the expression vector for Raftlin$^{YFP}$ and incubated with Texas Red-labeled poly(I:C). The subcellular localization and translocation of Raftlin$^{YFP}$ in response to poly(I:C) were almost similar to those observed with endogenous Raftlin (Fig. 4*E*). Notably, Raftlin$^{YFP}$ co-localized with Texas Red-poly(I:C) at the plasma membrane after 10-min incubation at 37 °C. Thereafter, poly(I:C) was internalized, spread to the endosomal compartments, and then accumulated in the organelles as shown in Fig. 3*A*. A membrane-associated Raftlin$^{YFP}$ appeared to move along with internalized poly(I:C) (Fig. 4*E*).

To clarify the function of Raftlin in poly(I:C) internalization mediated by clathrin, we examined physical association of F5 Raftlin with clathrin. As shown in Fig. 5, Raftlin did not interact with clathrin in unstimulated HeLa cells. When cells were stimulated with poly(I:C), Raftlin was co-immunoprecipitated with clathrin after a 10-min stimulation. However, after 30 min, Raftlin did not interact with clathrin any more. These results suggest that after poly(I:C) binding to the uptake receptor, Raftlin was recruited to the plasma membrane and associates with the clathrin complex to modulate cargo sorting and delivery.

*Raftlin Is Critical for Poly(I:C)-induced IFN-β Production in Human Myeloid DCs*—Human MoDCs expressed Raftlin but F6 not Raftlin-2 mRNA (Fig. 6*A*). When DCs were electrically transfected with siRNA for Raftlin, Raftlin expression was decreased compared with cells transfected with control siRNA (Fig. 6*B*, *right-hand panel*). Poly(I:C)-induced IFN-β mRNA expression was diminished in the Raftlin knockdown DCs (Fig. 6*B*, *left-hand panel*). The mRNA expression levels of TICAM-1, MDA5, and IPS-1 in Raftlin knockdown DCs were comparable with those in control DCs, although TLR3 expression was slightly reduced compared with control cells (Fig. 6*C*). Again, entry of poly(I:C) into Raftlin knockdown DCs was inhibited (Fig. 6*D*).

Raftlin was localized to both the plasma membrane and the cytoplasm of DCs (Fig. 6*E*, *upper panels*). Although membrane-associated Raftlin partially colocalized with CTXB, lipid raft disruption with MβCD in DCs did not affect poly(I:C) cellular ZSI uptake (supplemental Fig. S4). The mobilization of Raftlin in response to poly(I:C) was similar to that observed in HeLa cells (Fig. 6*E*, *lower panels*). After 30 min, Raftlin colocalized with TLR3 and Rab5 but not with LAMP1, indicating that Raftlin, together with the poly(I:C) uptake receptor, moves from the plasma membrane to the TLR3-positive early endosomes (Fig. 6*F*).

To determine the physiological function of Raftlin, we analyzed poly(I:C)-induced IFN-β production by BMDCs from wild-type or Raftlin$^{-/-}$ mice. Remarkably, wild-type and Raftlin$^{-/-}$ BMDCs expressed mouse Raftlin-2 mRNA at equivalent levels (Fig. 7*A*). There was no significant difference in F7 poly(I:C)-induced IFN-β production between wild-type and Raftlin$^{-/-}$ BMDCs (Fig. 7*B*). In addition, cellular uptake of poly(I:C) in Raftlin$^{-/-}$ BMDCs was comparable with that in wild-type BMDCs (Fig. 7*C*). To test the possibility that the Raftlin function is compensated with Raftlin-2 in Raftlin$^{-/-}$ BMDCs as observed in B cell receptor signaling in Raftlin$^{-/-}$ mouse B cells (33), we knocked down of mouse Raftlin-2 in Raftlin$^{-/-}$ BMDCs by infection with Raftlin-2 shRNA-expressing lentiviral particles and analyzed the cellular response to poly(I:C). Mouse Raftlin-2 expression was partially decreased in Raftlin$^{-/-}$ BMDCs (Fig. 7*D*, *right-hand panel*). Poly(I:C)-induced IFN-β mRNA expression was partially but significantly decreased in Raftlin-2 knockdown Raftlin$^{-/-}$ BMDCs (Fig. 7*D*, *left-hand panel*). Furthermore, internalization of Texas Red-labeled poly(I:C) was inhibited in ~40% of Raftlin$^{-/-}$ BMDCs infected with mouse Raftlin-2 shRNA lentiviral particles, reflecting the knockdown efficiency of mouse Raftlin-2 (Fig. 7*E*). These results suggest that mouse Raftlin-2 participates in poly(I:C) cellular uptake in Raftlin$^{-/-}$ BMDCs.

## DISCUSSION

Recent studies using mouse implanted tumor models indicate that poly(I:C) is a promising adjuvant for tumor vaccines because it promotes adaptive anti-tumor responses through the activation of myeloid DCs and induction of type I IFN production by multiple type of cells (10–15). However, it remains unresolved how poly(I:C) is delivered from the extracellular fluid to the intracellular poly(I:C) sensors localized on the endosomal membrane or cytoplasm.

In this study, we demonstrated that Raftlin is essential for poly(I:C)-induced cellular responses in human myeloid DCs and epithelial cells by mediating the cellular uptake of poly(I:C). Raftlin was originally identified as a major raft protein in B cells that co-localized with B cell receptor in the lipid raft before and after B cell receptor stimulation (29). However, subcellular localization of endogenous Raftlin appears to depend on the cell types. We found that in unstimulated HeLa cells, endogenous Raftlin localized diffusely in the cytoplasm and did not co-

FIGURE 6. **Raftlin is critical for poly(I:C)-induced IFN-β production in human myeloid DCs.** *A*, MoDCs express Raftlin but not Raftlin-2 mRNA. *B*, poly(I:C)-induced IFN-β production was decreased in Raftlin knockdown DCs (*left-hand panel*). Control and Raftlin knockdown DCs in a 24-well plate ($7 \times 10^5$/ml) were stimulated with 20 μg/ml of polymyxin B-treated poly(I:C) for 4 h. Total RNA was extracted and subjected to RT qPCR analysis for the expression of IFN-β. Data are representative of three separate experiments with similar results (mean ± S.D.). **, $p < 0.01$. Protein expression of Raftlin in DCs ($4 \times 10^5$) before and after siRNA transfection is shown (*B*, *right panel*). *C*, expression of TLR3, TICAM-1, MDA5, and IPS-1 in DCs. Total RNA from control and Raftlin knockdown DCs were extracted and subjected to RT-qPCR analysis for the expression of mRNA. Expression of each gene was normalized to GAPDH mRNA expression. *D*, uptake of Texas Red/poly(I:C) by MoDCs transfected with control siRNA (*upper panels*) or siRNA for Raftlin (*lower panels*). Control or Raftlin knockdown DCs were incubated with 40 μg/ml of Texas Red/poly(I:C) for 30 min at 4 °C. After washing, cells were incubated for up to 30 min at 37 °C. At the indicated periods, cells were fixed and visualized by confocal microscopy. Representative images from 20 fields in the indicated time points are shown. *Red*, Texas Red/poly(I:C); *blue*, nuclei with DAPI. *Bar*, 5 μm. *E* and *F*, confocal images of endogenous Raftlin in MoDCs in response to poly(I:C). *E*, *upper panels*, DCs were fixed and stained with anti-Raftlin pAb and Alexa 488/CTXB. *Red*, endogenous Raftlin; *green*, Alexa 488/CTXB; *blue*, nuclei with DAPI. *E*, *lower panels*, and *F*, DCs were incubated with 40 μg/ml of poly(I:C) as described in the legend to Fig. 4. At the indicated periods, cells were fixed and stained with anti-Raftlin pAb, anti-TLR3 mAb, anti-Rab5 mAb, or anti-LAMP1 mAb and Alexa Fluor-conjugated secondary Abs. Representative data from the indicated time points are shown. *Green*, endogenous Raftlin; *red*, TLR3, Rab5, or LAMP-1; *blue*, nuclei with DAPI. *Bar*, 5 μm.